Journal of South American Earth Sciences 36 (2012) 32–54

Contents lists available at SciVerse ScienceDirect

Journal of South American Earth Sciences

journal homepage: www.elsevier.com/locate/jsames

Petrology and geochemistry of Carboniferous siliciclastics from the Argentine Frontal Cordillera: A test of methods for interpreting provenance and tectonic setting

Luis A. Spalletti [a,d,*], Carlos O. Limarino [b,d], Ferrán Colombo Piñol [c]

[a] Centro de Investigaciones Geológicas, Calle 1, No. 644, B1900TAC, La Plata, Argentina
[b] Departamento de Geología, Facultad de Ciencias Exactas y Naturales, Universidad de Buenos Aires, Ciudad Universitaria, 1428 Buenos Aires, Argentina
[c] Departamento de Estratigrafía, Paleontología y Geociencias Marinas, Facultad de Geología, Universidad de Barcelona, C/Marti i Franqués s/n, E-08028 Barcelona, Spain
[d] Consejo Nacional de Investigaciones Científicas y Técnicas (CONICET), Argentina

ARTICLE INFO

Article history:
Received 9 February 2011
Accepted 15 November 2011

Keywords:
Carboniferous
Río Blanco Basin
Argentina
Sandstone petrology
Sedimentary geochemistry

ABSTRACT

Petrological and geochemical characteristics of sandstones and shales from the Carboniferous Cerro Agua Negra Formation (Río Blanco basin, western Argentina) are discussed. The sandstones are mostly feldspathic litharenites with subordinate litharenites and lithic arkoses, and their modal compositions indicate two major sources. The first represents a recycled orogen and can be identified as the Proto-precordillera, a N–S trending mountainous area that separated the Paganzo and Río Blanco basins and that was a positive element at least up until the end of the Carboniferous. The second was further east, in the Sierras Pampeanas terrane. It consisted of a variety of metasedimentary and felsic plutonic crystalline rocks. The Protoprecordillera must have been crossed by transverse valleys that facilitated the transfer of Pampean terrigenous material towards the Río Blanco basin. A lack of volcanogenic sand suggests that the basin was open towards proto-Pacific in the west, rather than being separated from it by a magmatic arc as previously suggested.

Bulk geochemical analysis of different lithological types (arenites, wackes and shales) demonstrates a strong relationship between texture and chemical composition of the rocks, even taking into account the immobile elements. The largest differences are between shales and arenites, while the wackes have intermediate compositions. The CIA (chemical index of alteration) indicates partial remobilisation of oxides from source rocks and enrichment of aluminium and potassium in the shales, which reflects their potassic clay mineral composition. Overall, siliciclastics of the Cerro Agua Negra Formation have a similar composition to the upper continental crust (with slight net enrichment of SiO_2 in the arenites and of Al_2O_3 in the shales). Rare earth element profiles reflect terrigenous contributions, since they are enriched in light-REE, have a pronounced negative Eu anomaly and a relative depletion of the heavy-REE. The results show that discrimination plots commonly employed to infer provenance and tectonic setting from siliclastics are compromised where bulk chemical composition is strongly dependent on grain size and sorting.

1. Introduction

Pioneering studies of the petrography and geochemistry of siliciclastic sedimentary rocks were performed by Maynard et al. (1982), Dickinson and Suczek (1979), Dickinson and Valloni (1980), Dickinson et al. (1983), McLennan et al. (1980), Taylor and McLennan (1981) and Floyd and Leveridge (1987). Subsequently, there have been many attempts to use sediment compositions as indicators of the siliciclastic provenance, dispersal, and the tectonic setting of source areas and their adjoining sedimentary basins. The chemical composition of sedimentary rocks is acknowledged to result from complex interactions between parent rocks, weathering, transport and diagenetic processes (McLennan, 1989; Cox and Lowe, 1996; Armstrong-Altrin et al., 2004). Nevertheless, some papers (e.g. Bhatia, 1983; Roser and Korsch, 1986) emphasised the relationships between geochemistry and provenance, or even between geochemistry and the tectonic context of deposition.

* Corresponding author. Centro de Investigaciones Geológicas, Calle 1, No. 644, B1900TAC, La Plata, Argentina.
E-mail addresses: spalle@cig.museo.unlp.edu.ar (L.A. Spalletti), limar@gl.fcen.uba.ar (C.O. Limarino), colombo@ub.edu (F.C. Piñol).

0895-9811/$ – see front matter © 2011 Elsevier Ltd. All rights reserved.
doi:10.1016/j.jsames.2011.11.002

Armstrong-Altring and Verma (2005) and Ryan and Williams (2007) have recently cautioned against the use of major element chemistry for such tectonic interpretations. In contrast, some trace elements (rare earth metals, Y, Th, Nb, Zr, Hf, Sc, etc.) that are not particularly mobile during weathering and diagenesis may reflect the characteristics of the source rocks more faithfully (Bhatia and Crook, 1986; McLennan, 1989; Armstrong-Altrin et al., 2004). All these contributions included interpretative chemical discrimination diagrams for the definition of provenance and for interpreting the tectonics of the source areas and sedimentary basins.

The aim of this study is to determine the origin and the tectonic context of Carboniferous siliciclastic rocks (the Cerro Agua Negra Formation) that are part of the record of the Río Blanco Basin. The strata crop out on the eastern flank of the Andes (Cordillera Frontal in Argentina) at a latitude of 30° south. The Cerro Agua Negra Formation is composed of arenites, wackes and shales. Modal analysis and bulk geochemistry reveal systematic differences between these rock types. These patterns are discussed and their significance evaluated in terms of the validity of compositional analysis for provenance and tectonic interpretations in siliciclastic successions.

2. Geological framework

The Andes extend as a continuous chain of mountains along the active (Pacific) margin of South America. This first-order orographic feature has its origin in the subduction of an oceanic plate underneath the continental South American plate. It can be divided into several tectonic segments characterised by different dip angles of the Benioff zone. Between 27° and 33° 30′ south, the Andes are in a segment of the Pampean flat-slab (Ramos et al., 2002) where there is considerable seismic activity, strong Pliocene–Quaternary uplift and significant Late Cenozoic magmatism. In a west–east cross section, different geological provinces can be recognised at this latitude (Fig. 1A): the Cordillera Principal, the Cordillera Frontal, the Precordillera and the Sierras Pampeanas (cf. Cahill and Isacks, 1992; Ramos et al., 2002).

The study area is situated in the eastern sector of the Cordillera Frontal at 30° S and 69° W (Fig. 1). The sedimentary rocks analysed, which form part of the fill of the Río Blanco Basin, are widely distributed throughout the region and constitute the type section of the late Pennsylvanian–early Cisuralian Cerro Agua Negra Formation (Aparicio, 1969; Polanski, 1970; González, 1977; Rodríguez Fernández et al., 1996; Césari and Gutiérrez, 2000; Limarino and Spalletti, 2006). This comprises >2000 m of siliciclastic sedimentary rocks, which have been substantially deformed by Gondwanan (Permian) and Andean (Cenozoic) orogenies (Rodríguez Fernández et al., 1996, 1999; Heredia et al., 2002; Busquets et al., 2005). The Cerro Agua Negra Formation unconformably rests on a series of Devonian greywackes and shales (Chigua Formation) which display a low-grade metamorphism that mainly affected the finest rock types.

Despite considerable deformation of the Upper Palaeozoic succession, it is possible to recognise eight informal lithostratigraphic sections in the study area (Fig. 2):

1) At the base of the Formation is a 200 m thick succession of poorly sorted and massive diamictites, lenticular sandstone bodies (some amalgamated and others separated by thin shaly-partitions), laminated mudstones, pebbly shales with dropstones, and intraformational conglomerates. This unit is interpreted as the deposit of a fan delta system related to a glaciated area that can be assigned to the Pennsylvanian glaciation (Pérez Loinaze et al., 2010).
2) A 150 m thick heterolithic succession is characterised by couplets of medium- to fine-grained sandstones and shales. These deposits commonly show all the features of low-density turbidity current deposits, such as normal graded and ripple-cross laminated sandstone beds with intraclasts and sole marks at their bases. Fairly thick packages can also be identified in which shales and grey dark mudstones are dominant.
3) A highly deformed section about 300 m thick and dominated by dark shales with localised thin layers of fine- and very fine-grained greywackes. Sandstone beds become more frequent near the top of this interval, resulting in a general upward coarsening trend. This interval represents the climax of the Gondwanan "postglacial transgression" and is characterised by the presence of the *Levipustula* fauna (Limarino et al., 2002).
4) A 70 m thick section of fluvial strata is developed above a regional unconformity and represents a basinward shift in the depositional systems. It consists of amalgamated lenticular sandstone bodies with abundant fragments of logs, and thin intercalations of organic-rich shales bearing abundant plant debris. The fossil plants of this succession are typical elements of the *Nothorhacopteris* palaeoflora and can be attributed to the megafloristic NBG Biozone (Archangelsky et al., 1987).
5) A 250 m thick heterolithic marine succession that consists of couplets of shales and very fine-grained sandstones with typical wave ripple cross-lamination, defining intervals of lenticular and wavy bedding (Reineck and Wunderlich, 1968). Throughout this section, there are also intervals that are entirely fine-grained, consisting of dark grey and black mudstones and shales. The succession corresponds to a short-lived marine transgression that occurred between the post-glacial flood event and the major latest Pennsylvanian transgression. A corresponding marine incursion is identified in the Carboniferous record of the neighbouring Paganzo basin (Limarino et al., 2006; Desjardins et al., 2009).
6) An 80 m thick section composed of multistorey fine-grained sandstone beds showing horizontal lamination, wave ripple cross-lamination and syneresis cracks in very thin pelitic partitions. Towards the top of the succession intercalations of medium-grained sandstones in large-scale trough and planar cross-stratified sets are more common. These also contain traces of *Palaeophycus* and *Planolites*. The upward coarsening suggests that accumulation occurred during progradation of a shoreface system.
7) A regional transgressive surface is succeeded by 120–130 m of dark fissile shales generated in an offshore marine environment and assigned to the Stephanian or late Pennsylvanian transgression.
8) The final 80 m thick unit consists of pebbly- to fine-grained sandstones and shales arranged in 0.3–1 m thick normal graded couplets. The sandstone beds commonly show abundant sole marks and a well-developed mud-chip intraformational conglomerate of rip-up clasts. In some instances the mudstones were eroded away during deposition of the overlying sandstone layer. All these features suggest deposition from repeated turbidity currents.

3. Study methods

The eight stratigraphic sections of the Cerro Agua Negra Formation were systematically sampled along the Agua Negra and the Arrequintín valleys (Fig. 2). Twenty-five sandstone samples and sixteen shale samples were collected. Sandstones were studied using standard thin-section petrographic analysis, and 300 grains per sample were point-counted, using the Gazzi-Dickinson method

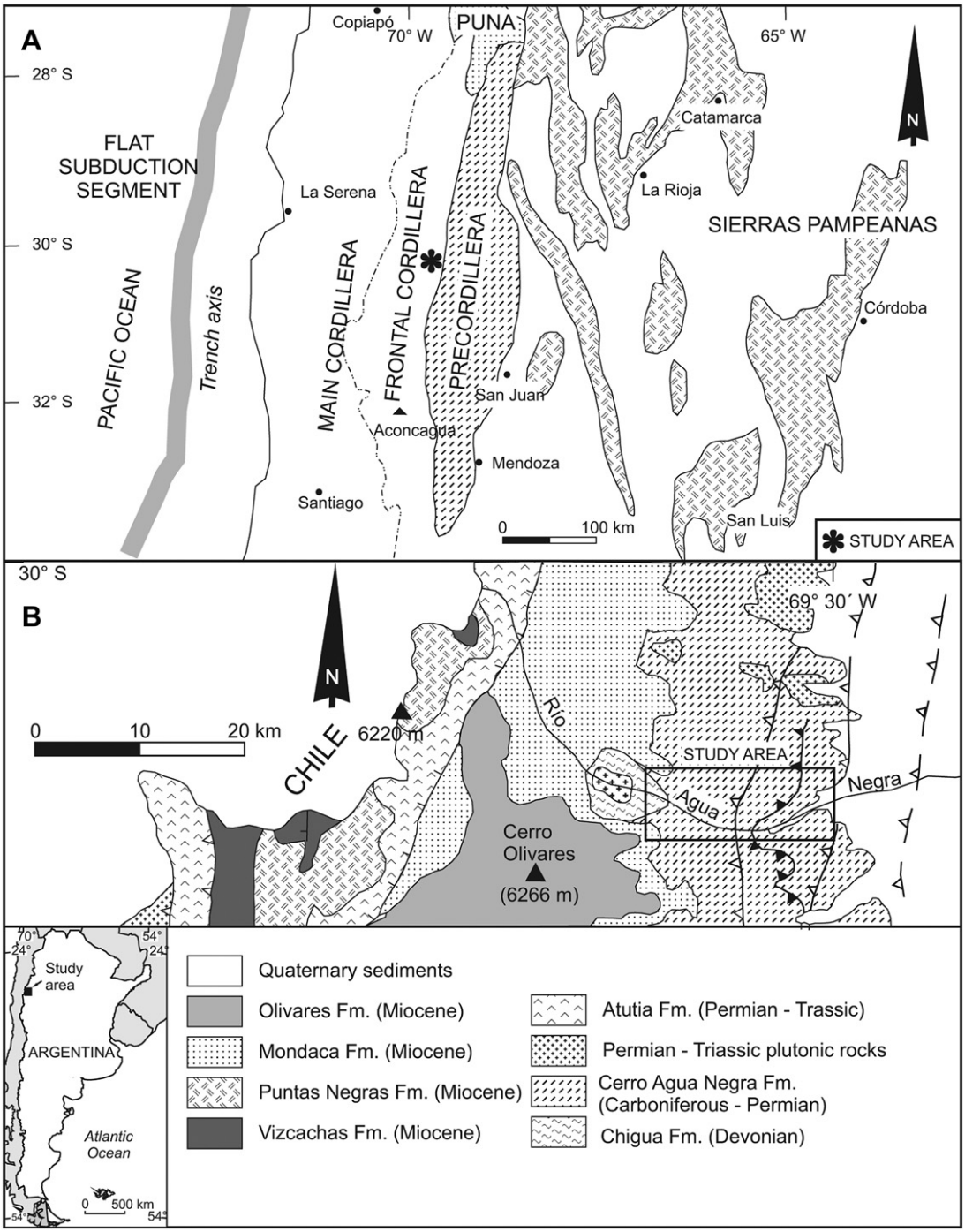

Fig. 1. A: map showing the flat-slab segment in the Central Andes and the main geologic provinces of the region (modified from Cahill and Isacks, 1992). B: geology of the study region (from Heredia et al., 2002).

in order to minimize the effect of the grain size on the modes (Gazzi, 1966; Dickinson, 1970).

The clay mineralogy of shales and wackes was determined by means of X-ray diffraction (XRD) analysis. For this study oriented aggregates of the <2 μm fraction were prepared by sedimentation onto glass slides and the clay mineral aggregates were examined in a PANalytical X′Pert PRO diffractometer equipped with a Cu target tube (1.54λ). Samples were analysed from 2 to 37° 2θ angle. The method of Chung (1974) and Moore and Reynolds (1989) was used for quantitative estimation of each identified mineral.

The geochemical study was performed on a 41 samples (16 shales, 13 wackes and 12 arenites). The samples were cleaned, and weathered coats and vein surfaces were cut off. The rocks were crushed to pieces <4 mm using a jaw crusher and then milled in a widia dish to a very fine powder, therefore W values were not considered in the present study. Loss on ignition was determined by heating the dried samples up to 950 °C for 2 h. To prepare fusion discs, each sample powder was mixed with a mixture of lithium tetraborate and lithium metaborate. The full bulk rock chemistry (both trace and major elements) was determined by Actlabs

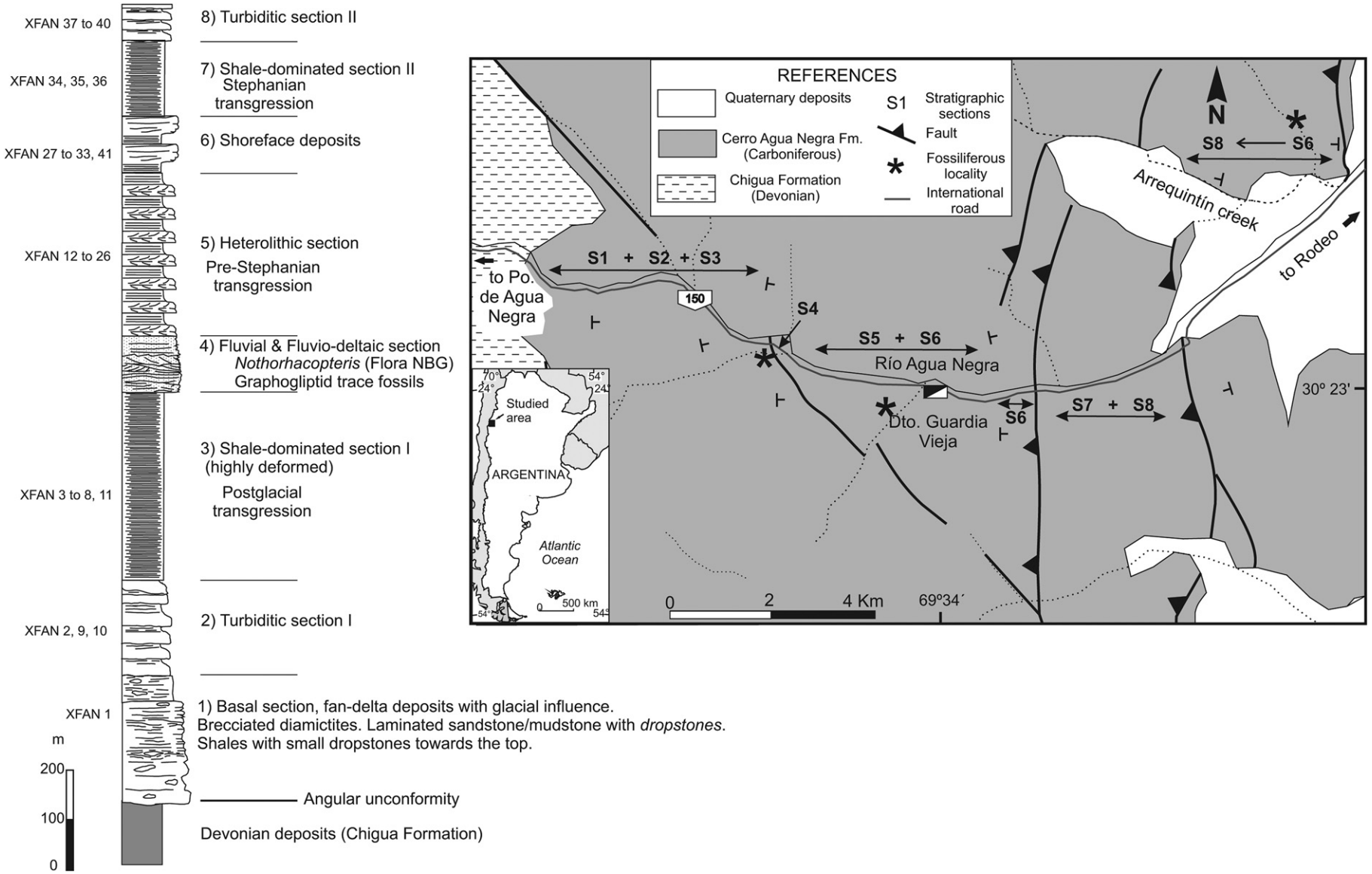

Fig. 2. Geological map of the Quebrada de Agua Negra valley and general stratigraphic section of the Cerro Agua Negra Formation with location of the samples studied.

(Canada) through the lithogeochemical method 4-Litho (details in http://www.actlabs.com).

4. Sandstone petrography

The results of the petrographic analysis of the sandstones from the Cerro Agua Negra Formation are given in Table 1. Monocrystalline (Qm) and polycrystalline quartz grains were detected, the latter of both sedimentary (Qps) and metamorphic origin (Qpm). Metamorphic quartz is mostly from mylonites and ultramylonites (Fig. 3a). Potassic feldspar varieties are orthoclase (FKo) and microcline (FKmic, Fig. 3b), and plagioclase grains identified were oligoclase to andesine with zonation (Plagz) and without zonation (Plag, Fig. 3c). The percentages of clasts showing well-developed patch perthite in orthoclase (Fig. 3d) or symplectitic textures in plagioclase (Fig. 3e) were calculated.

The lithic fragments were subdivided into volcanic (Lv), low-grade metamorphic rocks (Lmb) which are mainly slates and fine-grained schists (Fig. 3b and f), medium- and high-grade metamorphic rocks (Lma) which range from amphibolites to gneisses, and sedimentary rocks (Ls) which are mainly mudrocks and rare fragments of limestone and very fine-grained sandstone (Fig. 4b). The main accessory mineral grains are micas (biotite and muscovite), amphiboles and pyroxenes.

With the aim of producing regeneration diagrams of detrital modes (see Scasso and Limarino, 1997; Critelli and Ingersoll, 1996; Barone et al., 2008) the percentage of minerals greater than 62 microns was calculated, following the Gazzi-Dickinson method, and the results are shown in Table 1. The detrital modes clearly reflect the net dominance of lithoclasts over feldspars and a discrete proportion of quartz. Most of the sandstones studied are feldspathic litharenites. These sandstones show a high degree of

Table 1
Detrital modes of the sandstones from the Cerro Agua Negra Formation. A: modal components identified. B: modal composition of the sandstones and values of the index of compositional maturity.

A

	XFAN1	XFAN2	XFAN5	XFAN9	XFAN10	XFAN12	XFAN15	XFAN17	XFAN18	XFAN31	XFAN34	XFAN35	XFAN37	XFAN38	XFAN39	XFAN41
Qm	41	54	36	45	30	51	31	42	47	52	42	46	40	45	36	59
Qps	0	0	1	0	0	0	0	0	0	1	0	<1	0	0	1	0
Qpm	5	2	9	2	0	8	7	4	3	2	7	5	1	2	1	2
Qmb	1	1	0	4	1	0	0	0	0	0	0	0	0	1	0	0
Qma	1	0	2	1	2	3	1	0	1	2	0	0	0	2	0	1
Qv	0	0	1	0	0	0	1	0	0	0	1	0	0	0	1	0
FKo	9	9	9	7	11	5	10	16	12	12	10	9	11	5	6	10
FKop	6	6	5	4	4	3	6	1	4	6	6	3	3	1	3	4
FKm	1	0	1	2	1	0	1	0	0	1	<1	1	0	0	1	0
FKmb	0	0	0	0	0	0	0	0	0	0	0	0	0	0	0	0
FKma	0	0	0	0	0	0	0	1	0	1	0	0	0	0	0	0
FKv	0	0	0	0	0	0	0	0	0	0	0	0	0	0	0	0
Plg	6	5	11	7	2	<1	9	6	8	6	3	2	5	2	1	1
Plgmb	0	1	0	1	0	0	0	0	0	0	0	0	0	0	0	0
Plgma	1	1	1	1	1	0	0	0	0	0	0	0	0	1	0	0
Plgv	0	0	0	0	0	0	1	0	0	0	1	1	0	0	0	1
B-Mmb	1	<1	<1	0	4	<1	<1	12	2	0	1	3	8	0	7	1
B-Mma	0	0	0	0	0	0	<1	0	0	0	1	0	1	0	2	1
B-Mv	0	0	0	0	0	0	0	0	0	0	0	0	0	0	0	0
A-Pmb	0	<1	0	0	0	<1	<1	0	0	0	<1	<1	<1	0	0	<1
A-Pma	<1	0	0	0	<1	0	0	0	0	0	0	0	0	0	0	0
A-Pv	0	0	0	0	0	0	0	0	0	0	0	0	0	<1	0	0
Lm + Ls	24	20	23	26	43	30	31	18	23	17	24	30	31	40	39	19
Lv	4	1	1	<1	<1	0	2	0	<1	0	4	0	<1	<1	2	1

B

Sample	Q:F:Li	FK/Plg	Lv/Lt	CMI
XFAN 1	48:23:29	2.29	0.14	0.89
XFAN 2	57:22:21	2.14	0.05	1.33
XFAN 5	49:26:25	1.25	0.04	0.96
XFRAN 9	52:22:26	1.44	0.04	1.08
XFAN 10	33:19:48	5.33	0.02	0.52
XFAN 12	62:08:30	8.00	0	1.63
XFAN 15	40:27:33	1.70	0.06	0.67
XFAN 17	46:24:30	1.09	0	6.00
XFAN 18	51:24:25	2.00	0.04	1.09
XFAN 31	57:26:17	3.33	0	1.33
XFAN 34	50:20:30	4.00	0.17	1.04
XFAN 35	51:16:33	4.33	0	1.11
XFAN 37	41:19:40	2.80	0.03	0.82
XFAN 38	50:09:41	2.00	0.03	1.00
XFAN 39	39:11:50	10.00	0.05	0.75
XFAN 41	62:16:22	7.00	0.05	1.72

Qm: monocrystalline quartz; Qps: policrystalline quartz (chert); Qpm: policrystalline quartz (milonites); Qmb: quartz in low-grade metamorphics; Qma: quartz in high-grade metamorphics; Qv: quartz in volcanic rocks; FKo: orthoclase; FKop: pertitic orthoclase; Fkm: microcline; FKmb: othoclase in low-grade metamorphics; FKma: othoclase in low-grade metamorphics; FKv: K-feldspar in volcanic rocks; Plg: plagioclase; Plgmb: plagioclase in low-grade metamorphics; Plgma: plagioclase in high-grade metamorphics; Plgv: plagioclase in volcanic rocks; B-Mmb: micas in low-grade metamorphics; B-Mma: micas in high-grade metamorphics; B-Mv: micas in volcanic rocks; A-Pmb: amphibol & pyroxene in low-grade metamorphics; A-Pma: amphibol & pyroxene in high-grade metamorphics; Lm: metamorphic rock fragments; Ls: sedimentary rock fragments; Lv: volcanic rock fragments.CMI (compositional maturity index) = (monocrystalline quartz + policrystalline quartz)/(feldspars + rock fragments).

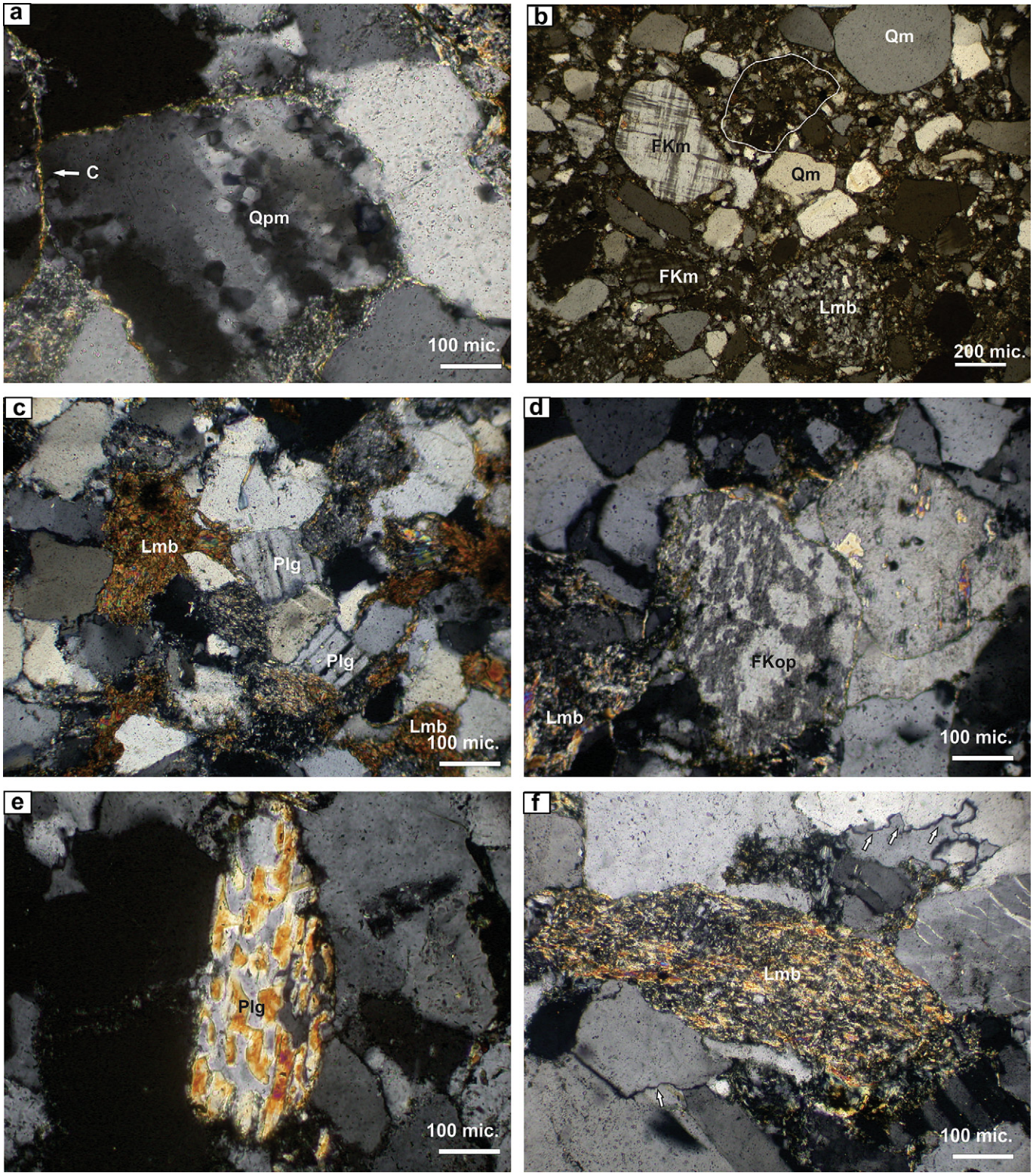

Fig. 3. a: Polycrystalline quartz grains (Qpm) interpreted as derived from mylonites; note the presence of chlorite cement forming rims (C). b: clasts of microcline (FKm), monocrystalline quartz (Qm) and low-grade quartzose schist (Lmb) in a sandstone showing large amounts of pseudomatrix (the white area shows the outline of a deformed clast). c: low-grade schist fragment (Lmb) and twinned plagioclase (Plg). d: clasts of perthitic orthoclase (FKop) interpreted as derived from crystalline rocks together with a schist fragment (Lmb). e: plagioclase grain (Plg) exhibiting symplectitic texture with biotite. f: large schist fragment (Lmb), arrows indicate partial dissolution of quartz clasts. All the photographs taken with crossed polars.

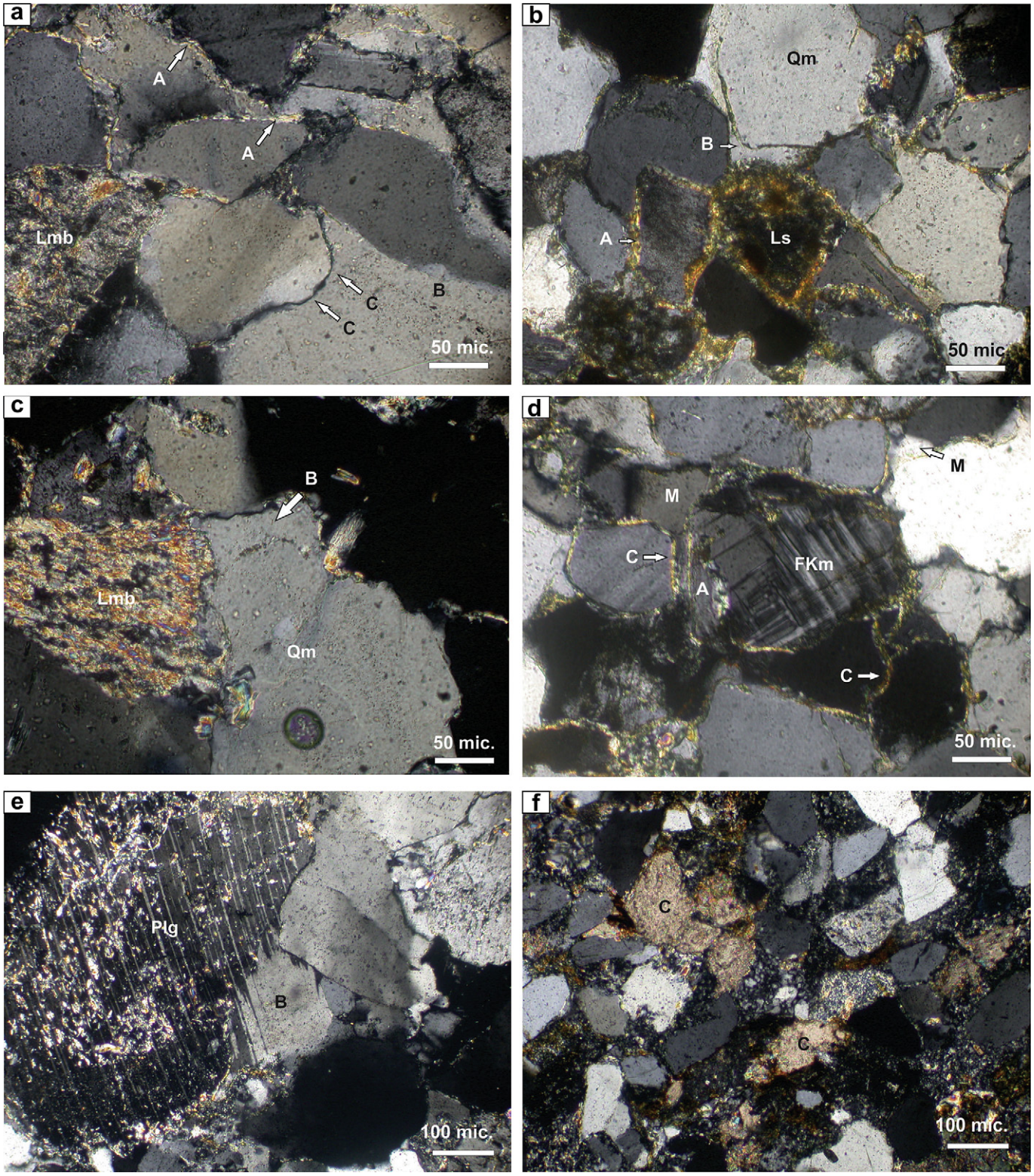

Fig. 4. a: Chlorite forming rim-type cement (A) and quartz overgrowths (B), note that chlorite cement is absent in zones where previously formed quartz overgrowths closed the intergranular space (C), Lmb indicates a low-grade schist fragment. b: chlorite rim-type cement (A) along sedimentary rock fragments (Ls) and quartz overgrowths (B) arranged over a monocrystalline quartz grain (Qm). c: well-developed quartz overgrowth (B) over a monocrystalline quartz clast (Qm), note that the quartz overgrowth is interrupted in the contact with a schist rock fragment (Lmb). d: K-feldspar (microcline, FKm) showing overgrowths (A) and later formation of chlorite cement (C), patches of megaquartz appear as later cement (M). e: plagioclase overgrowths (B) showing crystallographic inversion of the twinning, note the different alteration grade of the plagioclase grain (Plg) and the overgrowth (B). f: selective replacement of low-grade schist and sedimentary rock fragments by calcite (C), this process was only identified in matrix-rich sandstones. All the photographs taken with crossed polars.

mechanical compaction (in some cases with the development of a pseudomatrix from compacted clay-rich lithoclasts, Fig. 3b) and various types of cement, including syntaxial quartz overgrowths (Fig. 4a–c), megaquartz (Fig. 4d), chlorite (Fig. 4a, b and d), feldspar overgrowths (Fig. 4d and e) and calcite (Fig. 4f).

Monocrystalline quartz grains always outnumber those of polycrystalline quartz, both the Qps and of the Qpm types (Table 1). Lithoclasts of metamorphic and sedimentary origin are the most abundant type and volcanic examples are rare. The most frequent feldspar grains are potassium varieties, in particular orthoclase (between 6% and 18%). Plagioclase never accounts for more than 11% of the total proportion of grains and they are usually less than 7 modal %.

The low proportion of detrital quartz, the freshness of feldspars (especially plagioclase) and the very low values for the index of compositional maturity (ratio of total quartz to the feldspars and metastable lithoclasts, Table 1B) indicate a very short residence time of the clastic material in the weathering–transport–deposition system. It suggests the existence of high topographic relief in the source areas, a relatively short transportation distance, and rapid burial in a strongly subsiding basin.

5. Sandstone provenance

The best indicators of source rocks for the Cerro Agua Negra Formation are the lithic clasts. Low-grade metamorphic rock grains (schists and phyllites) and siliceous sedimentary rocks (siltstones, very fine-grained sandstones) can be identified. Volcanic rock fragments (mainly showing felsitic and porphiritic textures) are scarce (Table 1).

Two varieties of polycrystalline quartz can be distinguished, microgranular grains of siliceous sedimentary rocks (chert) and mosaics made up of several elongated crystals (normally more than five) with sutured intercrystalline contacts from low- to moderate-grade metamorphic rocks (Blatt et al., 1980; Asiedu et al., 2000). Monocrystalline quartz grain have equant shapes, variable extinction (with predominance of moderately undulose extinction), and are limpid or with acicular rutile micro-inclusions. These attributes suggest that the monocrystalline quartz originated from upper crustal, granitic and/or high-grade metamorphic rocks (Tortosa et al., 1991; Jafarzadeh and Barzi, 2008).

The predominant K-feldspars include grains of orthoclase (with a high degree of alteration) and microcline (slightly altered). Orthoclase is both monocrystalline, Carlsbad twinned, or perthitic. These types of K-feldspars indicate an upper crustal origin, essentially from felsic plutonic rocks. The plagioclases (oligoclase to andesine) are small, clean grains with a low degree of alteration. Some of the grains show normal growth zonation. These features also suggest that plagioclase was derived from plutonic rocks (Pittman, 1963) although a potential contribution from metamorphic rocks cannot be ruled out (Höy, 1976).

In the Dickinson et al. (1983) provenance diagram the majority of the detrital modes are located in the mixed sector (Fig. 5A). Nevertheless, the abundant grains of low-grade metamorphic rocks and highly altered sedimentary rocks indicate contributions from a recycled orogen (Dickinson et al., 1983). Additionally, common monocrystalline equant quartz grains with undulose extinction, and the presence of perthitic orthoclase and microcline indicate contributions from crystalline upper crustal rocks with felsic composition. All these parent lithologies are presently exposed in the Precordillera region, particularly the western Precordillera (siliciclastic sedimentary units from the Lower Palaeozoic, in part showing evidence of low-grade metamorphism) and the Sierras Pampeanas (with important upper crustal granitoid rocks).

These interpretations support the existence of an uplifted terrane to the east of the Río Blanco basin. This is designated the "Protoprecordillera" (Amos and Rolleri, 1965) and is a typical recycled orogen that constituted a north–south oriented topographic high which geographically separated the Río Blanco and the Paganzo basins in the Carboniferous (Fig. 6) (Salfity and Gorustovich, 1983; Limarino et al., 2006; Fielding et al., 2008; Henry et al., 2008). Moreover, evidence of contributions from the Sierras Pampeanas to the Rio Blanco Basin implies sediment transport from regions even further east than the Protoprecordillera, which must therefore have been dissected by transverse E–W valley systems (cf. Fig. 6).

To evaluate the relative contribution from these source areas, three petrosomes (used to describe consanguineous regionally correlatable units, Ingersoll and Cavazza, 1991) have been defined that include the petrofacies derived from the major morphostructural elements (Net and Limarino, 2006): 1) Protoprecordilleran orogen (PO), 2) Pampean terrain (PT) and 3) Protoprecordilleran volcanism (PV) (Table 2). The average modal composition corresponds to $PO_{70}PT_{25}PV_4$ and indicates an

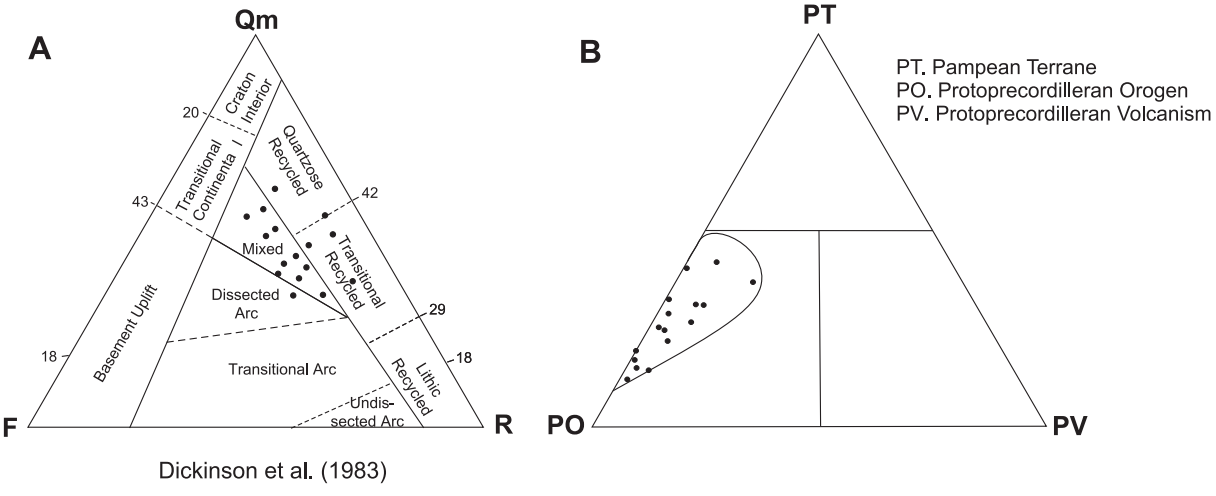

Fig. 5. Detrital modes and ternary diagrams for sandstone samples from the Cerro Agua Negra Formation. A: Folk et al. (1970) classification, B: provenance diagram of Dickinson et al. (1983), C: distribution of the three petrosomes defined in the present study.

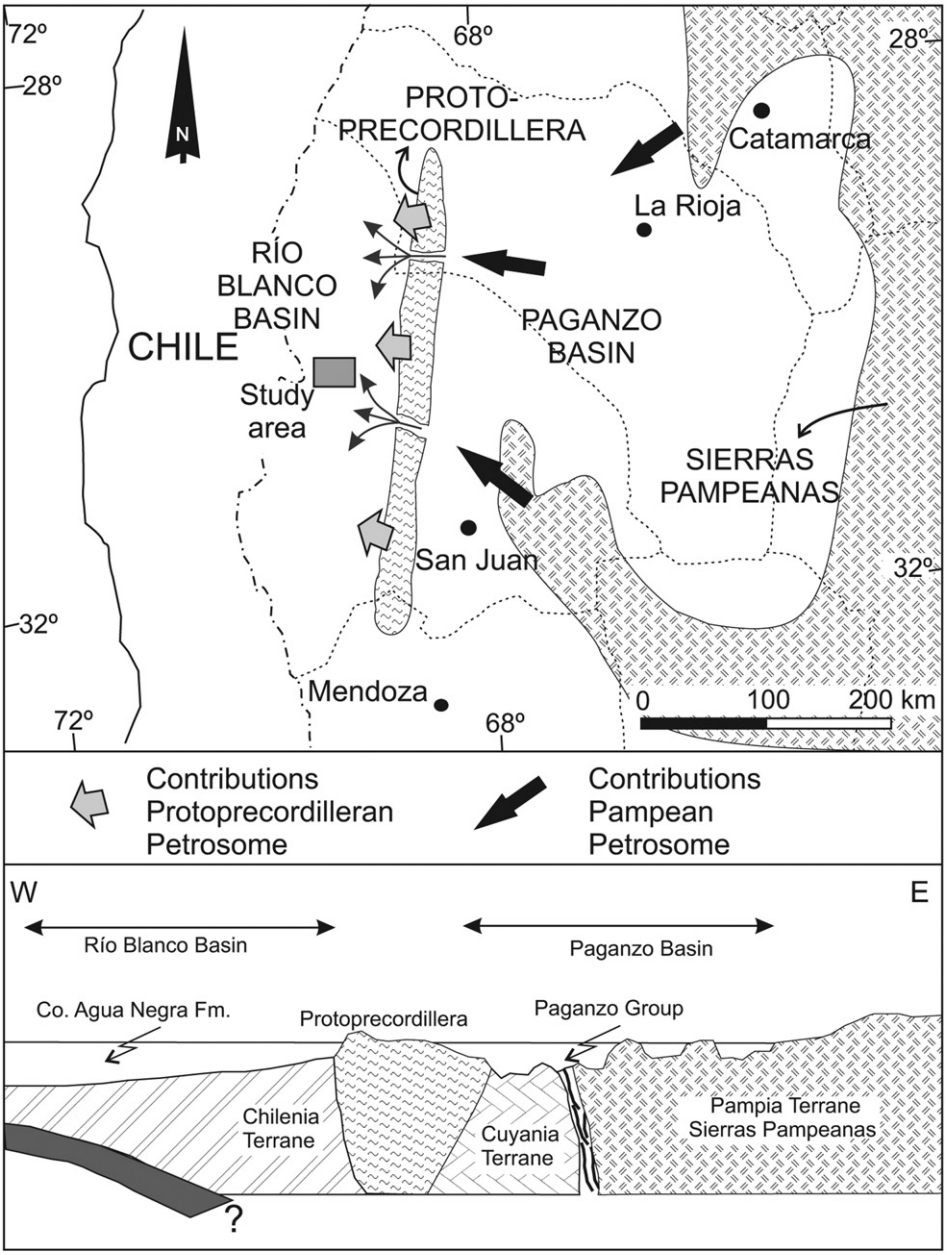

Fig. 6. Palaeogeographic reconstruction showing the location of the Paganzo and the Río Blanco basins, and the Protoprecordillera and Sierras Pampeanas source areas. The arrows show the most important transport directions for siliciclastic materials of the Cerro Agua Negra Formation. The lower part shows a schematic E–W section of the provenance areas, the Upper Palaeozoic sedimentary basins and the location of the allochthonous blocks (Pampia, Cuyania and Chilenia) accreted on the western margin of Gondwana during the Lower Palaeozoic.

important contribution of the Protoprecordilleran orogen (Fig. 5B), with moderate contributions from the components of the Pampean terrain and a much lesser proportion from Protoprecordilleran volcanism (Fig. 5B). Relative homogeneity in the sandstone petrology and mineral composition suggests that provenance, transport and depositional conditions remained approximately constant during accumulation of the Cerro Agua Negra Formation.

Table 2
Percentage values of the three petrosomes (Protoprecordilleran orogen, Pampean terrain and Protoprecordilleran volcanism) defined in this study.

	XFAN1	XFAN2	XFAN5	XFAN9	XFAN10	XFAN12	XFAN15	XFAN17	XFAN18	XFAN31	XFAN34	XFAN35	XFAN37	XFAN38	XFAN39	XFAN41
PO	60	69	53	74	84	68	62	83	73	60	47	77	87	83	81	67
PV	9	3	5	2	2	0	8	0	3	0	16	2	2	0	5	7
PT	31	28	42	24	14	32	30	17	24	40	37	21	11	17	14	26

Protoprecordilleran Orogen (PO) = Qpch + Qmb + FKmb + Plgmb + B-Mmb + Ls + Lm; Protoprecordilleran volcanism (PV) = Qv + FKv + Plgv + Lv; Pampean Terrane (PT) = Qpm + Qma + FKop + FKm + FKma + Plgma + B-Mma.

Table 3
X-ray diffraction data for the shales and wackes of the Agua Negra Formation (Fraction < 2 μm).

Sample	Rock type	Illite		Chlorite		I-S	Kaolinite		Quartz	Feldspar
		Content (%)	Crystallinity	Content (%)	Crystallinity		Content (%)	Crystallinity		
XFAN 3	Shale	75	Good	25	Good	t	t		a	p
XFAN 4	Wacke	75	Good	25	Fair	t			a	p
XFAN 8	Shale	80	Good	20	Good	t			a	p
XFAN 19	Shale	65	Good	35	Good	t			a	p
XFAN 21	Wacke	80	Good	10	Poor	t	10	Poor	a	p
XFAN 26	Shale	85	Good	15	Poor	t			a	p
XFAN 28	Wacke	75	Good	25	Fair	t			a	p

t: traces; a: abundant; p: poor.

6. X-ray diffraction analysis

The <2 μm fraction of seven selected samples is essentially composed of illite and chlorite, and randomly interlayered illite–smectite mixed-layer clays (Table 3). Illite has a good degree of crystallinity, whereas the chlorite crystallinity varies from poor to high. The quantitative analysis of clay minerals is fairly uniform and does not show major variations among samples (Table 3). The clay mineral assemblage is interpreted as the result of combination of a complex set of factors, such as source rock, climate, transport, and diagenesis. The variable degree of crystallinity of chlorite suggests that this clay mineral derived from previous pelitic and low-grade metamorphic rocks. Though illite may be also considered as detrital, its good degree of crystallinity and the presence of interlayered I-S clay indicate that at least part of the illite may be a product of mesogenetic transformation of smectite.

7. Sedimentary geochemistry

Chemical analyses of shales, wackes and arenites from the Cerro Agua Negra Formation are presented in the Appendix, and average values are summarised in Table 4 and plotted in Fig. 7. Major element compositions differ significantly between the rock types, mostly reflecting sand:clay proportions. Arenites have an average of 82.68% SiO_2, wackes have a lower content (average 68.35%) and the shales are the most silica-defficient (average 61.54%). The shales are richest in Al_2O_3, Fe_2O_3, MgO, K_2O and TiO_2, reflecting a clay fraction dominated by illite and chlorite. Another point worthy of note is that all sediments have similar contents of CaO and Na_2O (Fig. 7). Unsurprisingly, Fig. 7 also displays strong negative correlation between Fe_2O_3(t), TiO_2, Al_2O_3 and MgO versus SiO_2. The less predictable negative correlation between K_2O and SiO_2 may be due to the illite-rich composition of the shales, which outweighs higher K-feldspar contents of the arenites. Logarithmic relationships Fe_2O_3/K_2O and SiO_2/Al_2O_3 have been used by Herron (1988) as a basis for geochemical classification of siliciclastic rocks (Fig. 8). The majority of the Cerro Agua Negra samples correspond to their textural classification, although many of the shales plot in the wacke field and several wackes plot as more mature litharenites, because both rock types have more SiO_2 content relative to Al_2O_3 than expected.

Minor components and trace elements also vary between the discrete sedimentary rock types (Table 4). Shales have higher average values than the arenites for Sc, V, Ba, Y, Cr, Ga, Rb, Nb, Cs, La, Ce, Pr, Nd, Sm, Eu, Dy, Er, Yb, Th and U, while arenites have higher average values for Zr, Co, Ta and W. In all cases the wackes have the intermediate values for these elements, albeit nearer those of the shales than those of the arenites. However, wackes are the richest in Sr and Hf.

7.1. Geochemistry and weathering

Even when the chemical composition of siliciclastic sediments reflects that of the source rocks, it is may be modified by weathering and diagenetic processes (Boles and Franks, 1979; Nesbitt et al., 1996; McLennan, 2001). In many cases low-temperature diagenesis effectively continues the mineralogical stabilisation processes from the weathering zone. One of the parameters most often used to determine the degree of chemical weathering is the chemical index of alteration or CIA (Nesbitt and Young, 1982). This is defined as: $100 \times [Al_2O_3/(Al_2O_3 + CaO + Na_2O + K_2O)]$, and indicates the level of degradation of primary metastable and unstable minerals (for example, feldspars, heavy minerals and volcanic glass) into clay minerals.

The CIA may be represented via a ternary plot of Al_2O_3–$CaO + Na_2O$–K_2O (Fig. 9). For the Cerro Agua Negra Formation it shows that the largest values of CaO plus Na_2O are found in the least aluminous rocks, and that the most aluminous rocks have relatively higher levels of K_2O. The contents of $CaO + Na_2O$ and K_2O are always higher than the average for volcanic rocks (basaltic andesites, andesites and rhyolites). The elevated values of Al and K in the shales and wackes reflect the relative abundance of illite, while the comparatively higher

Table 4
Average chemical composition of shales, wackes and arenites from the Cerro Agua Negra Formation.

	SiO_2 (%)	Al_2O_3 (%)	Fe_2O_3(T) (%)	MnO (%)	MgO (%)	CaO (%)	Na_2O (%)	K_2O (%)	TiO_2 (%)	P_2O_5 (%)	Sc (ppm)	V (ppm)	Ba (ppm)	Sr (ppm)	Y (ppm)	Zr (ppm)	Cr (ppm)	Co (ppm)	Ga (ppm)
Shales	61.54	18.26	7.02	0.076	2.30	0.48	1.08	3.74	0.90	0.16	18.44	139	658	67	34	180	82	16	23
Wackes	68.35	15.01	4.83	0.078	1.52	1.01	1.76	2.69	0.74	0.14	14.00	101	532	116	31	223	58	23	18
Arenites	82.68	8.23	1.62	0.029	0.55	0.65	1.43	1.57	0.36	0.09	6.17	46	236	80	16	223	23	37	9

	Rb (ppm)	Nb (ppm)	Sn (ppm)	Cs (ppm)	La (ppm)	Ce (ppm)	Pr (ppm)	Nd (ppm)	Sm (ppm)	Eu (ppm)	Dy (ppm)	Ho (ppm)	Er (ppm)	Tm (ppm)	Yb (ppm)	Lu (ppm)	Hf (ppm)	Ta (ppm)	Tl (ppm)	Th (ppm)	U ppm
Shales	170	15	5	14	40	88	10	35	7	1.5	6.2	1.3	3.8	0.6	3.6	0.5	5.5	1.6	0.9	14.8	3.9
Wackes	126	12	5	10	35	74	9	30	6	1.4	5.6	1.2	3.48	0.5	3.3	0.5	6.6	2.0	0.9	12.3	3.4
Arenites	68	7	5	5	28	58	7	22	4	0.8	3.3	0.6	2.0	0.3	1.9	0.3	6.1	3.2	0.6	7.7	1.8

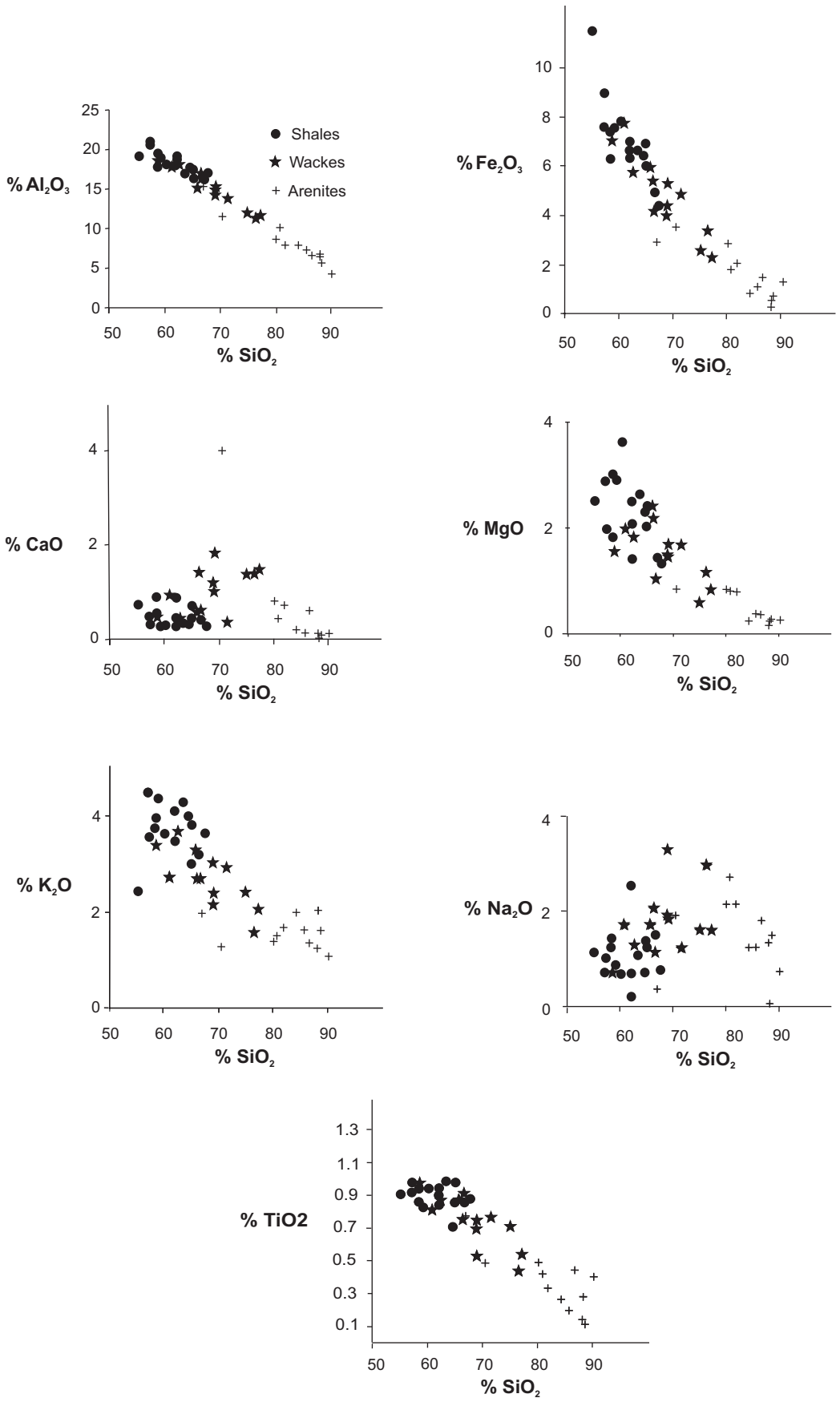

Fig. 7. Selected major element-SiO_2 plots for the arenites, wackes and shales of the Cerro Agua Negra Formation.

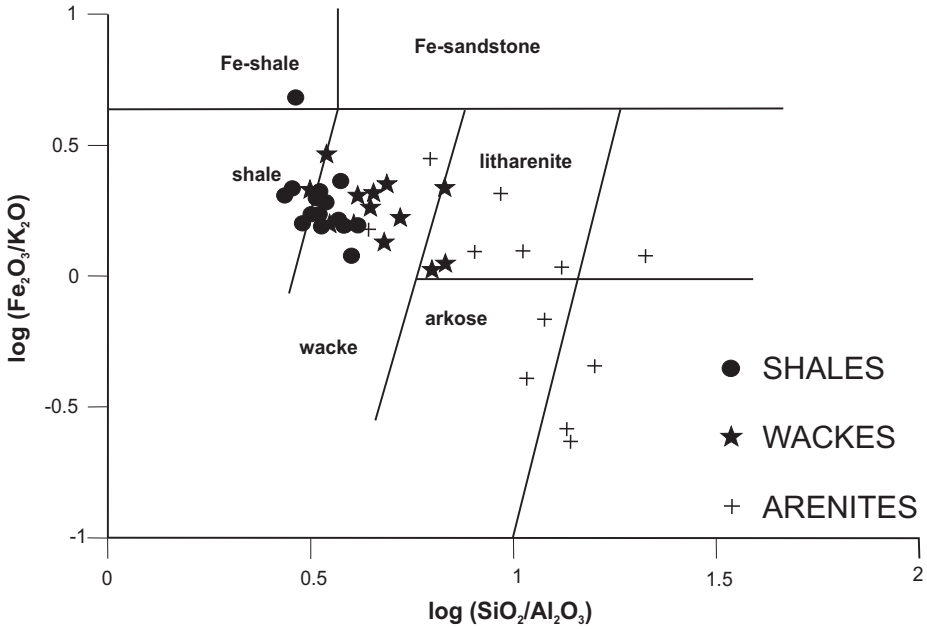

Fig. 8. Geochemical classification of the Cerro Agua Negra samples using the diagram log Fe_2O_3/K_2O vs. log SiO_2/Al_2O_3 (after Herron, 1988).

$CaO + Na_2O$ content in the arenites is due to the presence of relatively fresh plagioclase grains.

The CIA does not take into account silica contents, and the two parameters are broadly negatively correlated but with a wide scatter for arenites (Fig. 10). This suggests that the CIA is directly related to the amount of clay minerals in the rock. Thus, this index is a better proxy for alteration and/or mesogenetic precipitation of secondary minerals in clay-rich lithologies (wackes and mudrocks) than in arenites.

7.2. Geochemistry, provenance and tectonic interpretation

Following pioneering work of Taylor and McLennan (1981), McLennan and Taylor (1984, 1991), McLennan (1989), Taylor et al. (1986), Bhatia and Crook (1986), and Floyd and Leveridge (1987), bulk geochemistry of siliciclastic rocks has frequently been used to determine both provenance and tectonic context (of source areas and basins). A common approach compares the major element geochemistry with an average composition of upper continental crust (UCC, Taylor and McLennan, 1985). Applying this to the Cerro Agua Negra Formation (Fig. 11) it is apparent that several of the oxides that correspond to the major elements have lower values than those of the averages for the crust, in particular CaO and Na_2O. As should be expected due to the natural process of weathering and the increase in stable components in response to surface conditions, the arenites are enriched in SiO_2 (quartz), to the same extent as the shales are enriched in Al_2O_3 (secondary clay minerals). Among trace elements, the Agua Negra sediments are comparatively depleted in Sr (probably following CaO values), and have similar contents of Zr and Co. In the shales and wackes the concentrations of Sc, V, Ba, Y, Ga, Rb, Sn, Th and U are close to the UCC values, while these elements are comparatively depleted in the arenites (Fig. 11). In

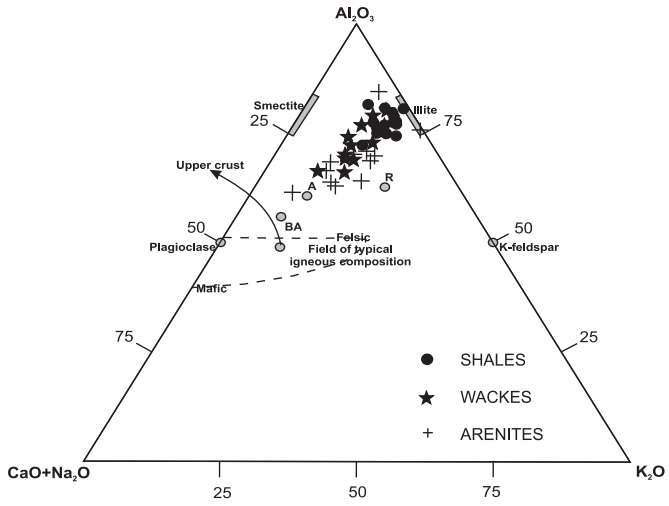

Fig. 9. Ternary diagram Al_2O_3–($Na_2O + CaO$)–K_2O. BA, basaltic andesite; A, andesite; R, rhyolite. The samples studied plot in the central field between feldspars and the clay minerals, and therefore they show a moderate degree of weathering.

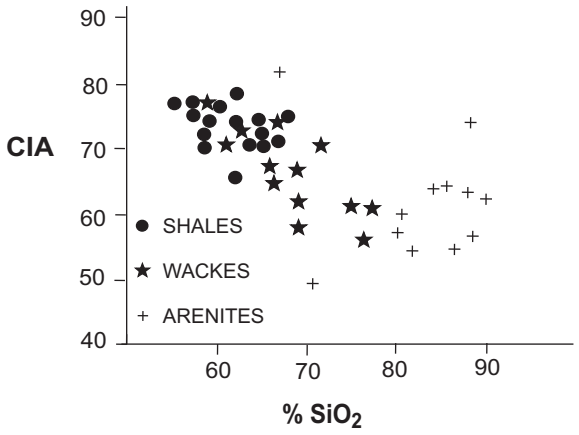

Fig. 10. Bivariate plot SiO_2 vs. CIA = $100 \times Al_2O_3/(Al_2O_3 + CaO + Na_2O + K_2O)$ (Nesbitt and Young, 1982) for the Cerro Agua Negra samples. Note the inverse relation between the two components.

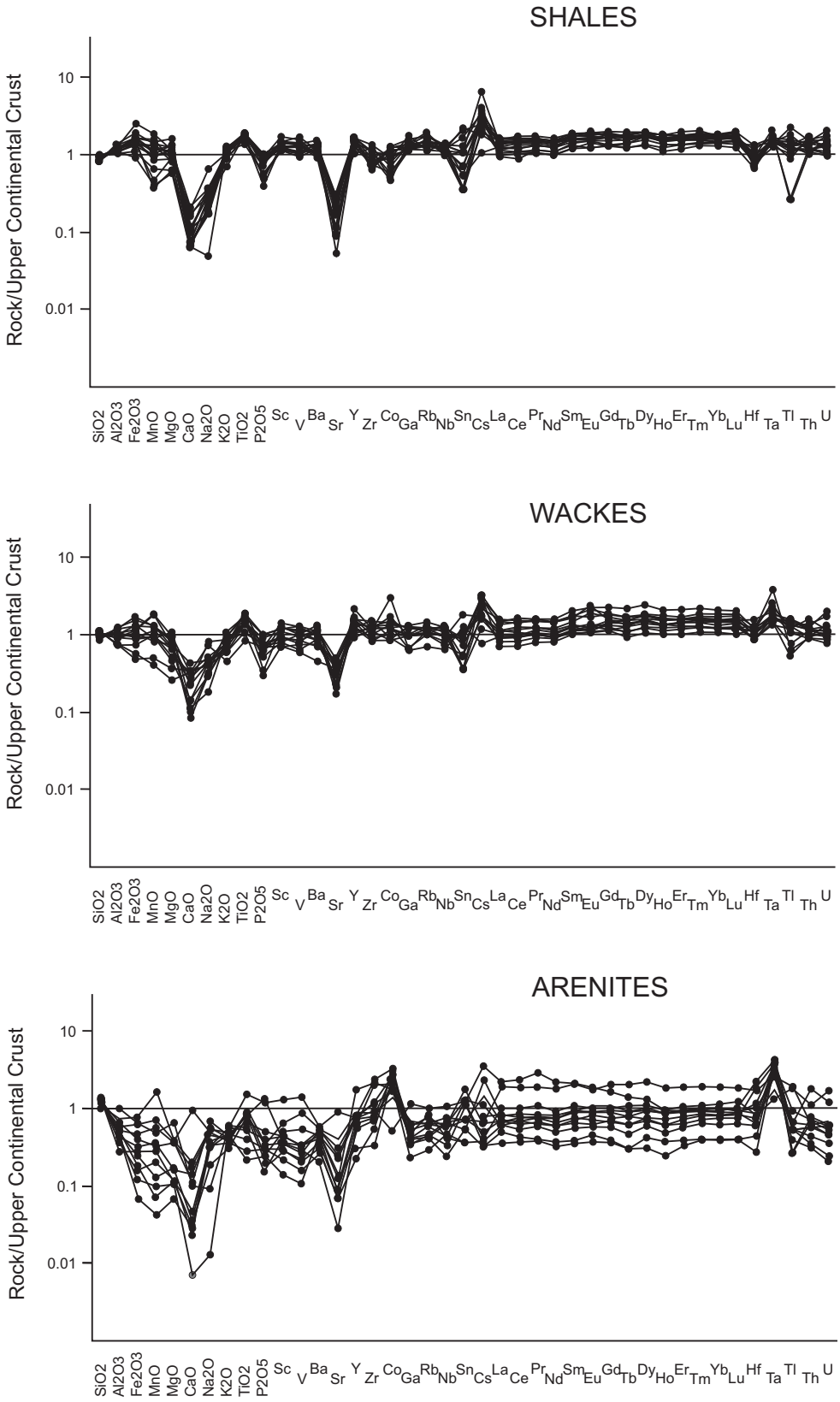

Fig. 11. Multi-element normalized diagram rock/upper continental crust for the different lithological types defined in the Cerro Agua Negra Formation.

the shales and in the wackes, the rare earth elements as a whole are higher than the average for the upper crust, while in the arenites there is a large spread of values above and below the continental crust averages.

REE concentrations in sedimentary rocks are also commonly compared to average chondritic values (Nakamura, 1974), as well as to post-Archean Australian shale (PAAS), which has been considered an average for terrigenous contributions Taylor and McLennan, 1985). The Cerro Agua Negra Formation samples have a similar REE profile to PAAS (Fig. 12), relative enrichment of the light rare earth elements, low values with a general flat geometry for the heavy rare earth elements, and a significant negative anomaly for Eu. Similar results were found in other studies by Floyd and Leveridge (1987); Asiedu et al. (2004) and Gu et al. (2002) and reflect a derivation from continental crust and/or continental magmatic arcs (cf. McLennan et al., 1993; Lamaskin et al., 2008). Compared to the clay-rich samples, arenites show a greater variability in REE enrichment ratios and a less marked Eu anomaly (Fig. 12), and this may be related to a sorting effect. There is a strong positive correlation between K and Rb contents in the Cerro Agua Negra Formation (Fig. 13), and the data range corresponds to intermediate to acid compositions (Floyd and Leveridge, 1987; Floyd et al., 1989, 1990). Shales are richest in K and Rb, reflecting the high proportion of illite in the clay mineralogy.

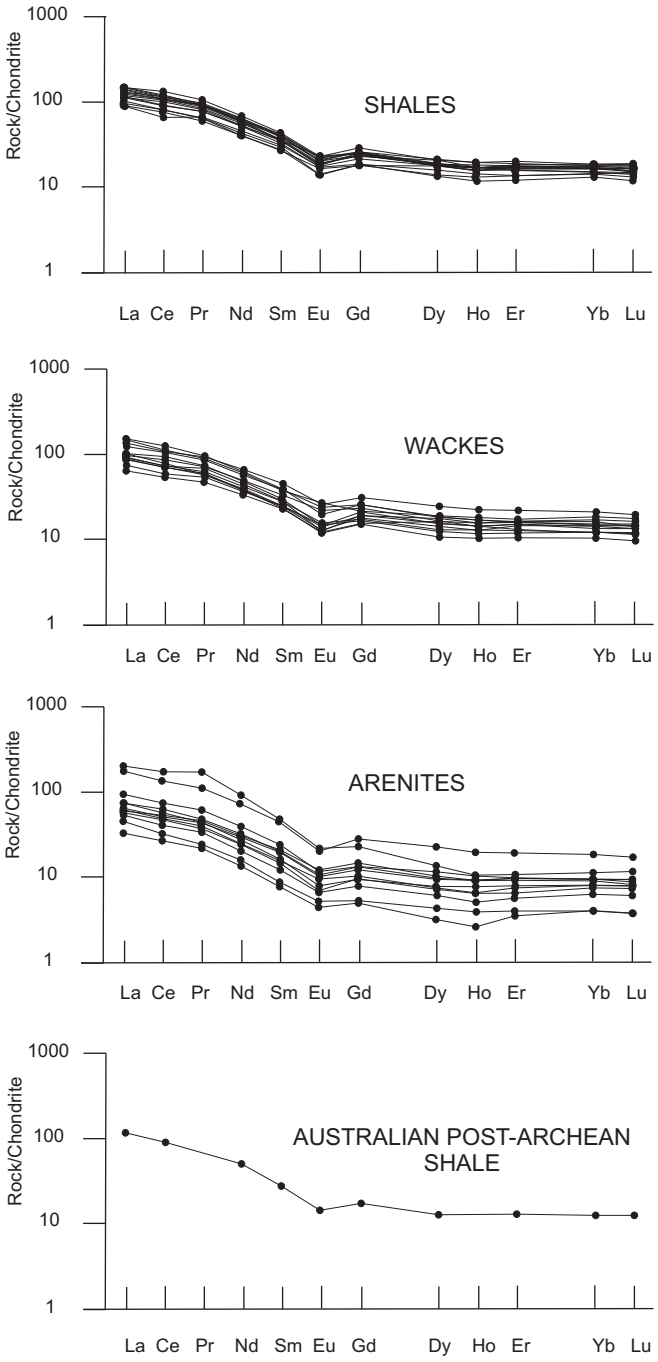

Fig. 12. Chondrite-normalized REE diagram for different types of sedimentary rocks of the Cerro Agua Negra Formation. Note the similar pattern between the samples studied and the PAAS.

The most important bulk geochemical interpretations of siliciclastic sedimentary rocks are based on the study of the "immobile" elements, such as Th, Sc, Hf, La and Zr (cf. Taylor and McLennan, 1985; Bhatia and Crook, 1986; McLennan et al., 1993; Roser et al., 1996; Vujovich and Kay, 1998). Other components are sensitive to remobilisation during processes of weathering, diagenesis and metamorphism. The analysed samples display a well-defined trend between the Zr/Sc ratio and SiO_2 (Fig. 14A). Zirconium is considered to be characteristic of upper crust rocks and highly resistant to alteration, whereas Scandium tends to be concentrated in mantle-derived mafic rocks and is more geochemically mobile. The trend in Fig. 14A therefore goes from less recycled (shales) to more recycled (arenites). Fig. 14B compares the Th/Sc and Zr/Sc ratios (McLennan et al., 1990, 1993). Th and Zr enrichments are typical of rocks from the upper crust and Zr increases with recycling relative to other more mobile elements. The shales and most of the wackes of the Cerro Agua Negra Formation plot in the area that corresponds to the UCC, while some of the wackes and especially the arenites are displaced towards the field of sedimentary recycling. It is likely that higher contents of Zr in the arenites are due to the tendency of physically robust zircons to constitute sand-sized grains.

The classic major element discrimination plots for determining the tectonic setting of terrigenous sedimentary rocks are shown in Figs. 15–18 (Roser and Korsch, 1986; Bhatia, 1983, Bhatia and Crook, 1986, Floyd and Leveridge, 1987). However they provide ambiguous results for the Cerro Agua Negra Formation. In the Al_2O_3/SiO_2 versus $Fe_2O_3 + MgO$ plot (Fig. 15A) and the TiO_2 versus

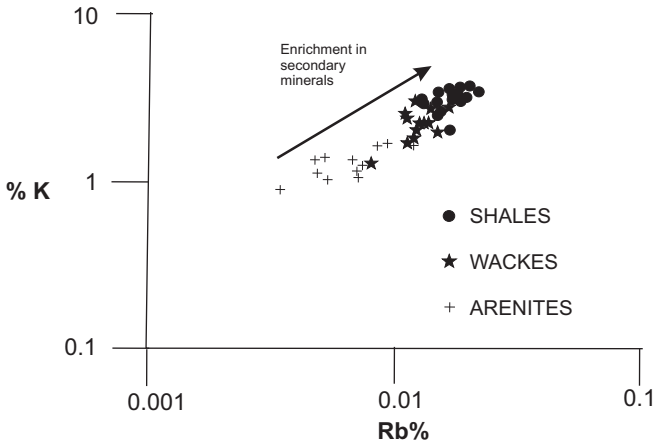

Fig. 13. Distribution of K and Rb in the Cerro Agua Negra sedimentary rocks. The higher values of K and Rb in the shales are attributed to the enrichment in weathering products and secondary clay minerals.

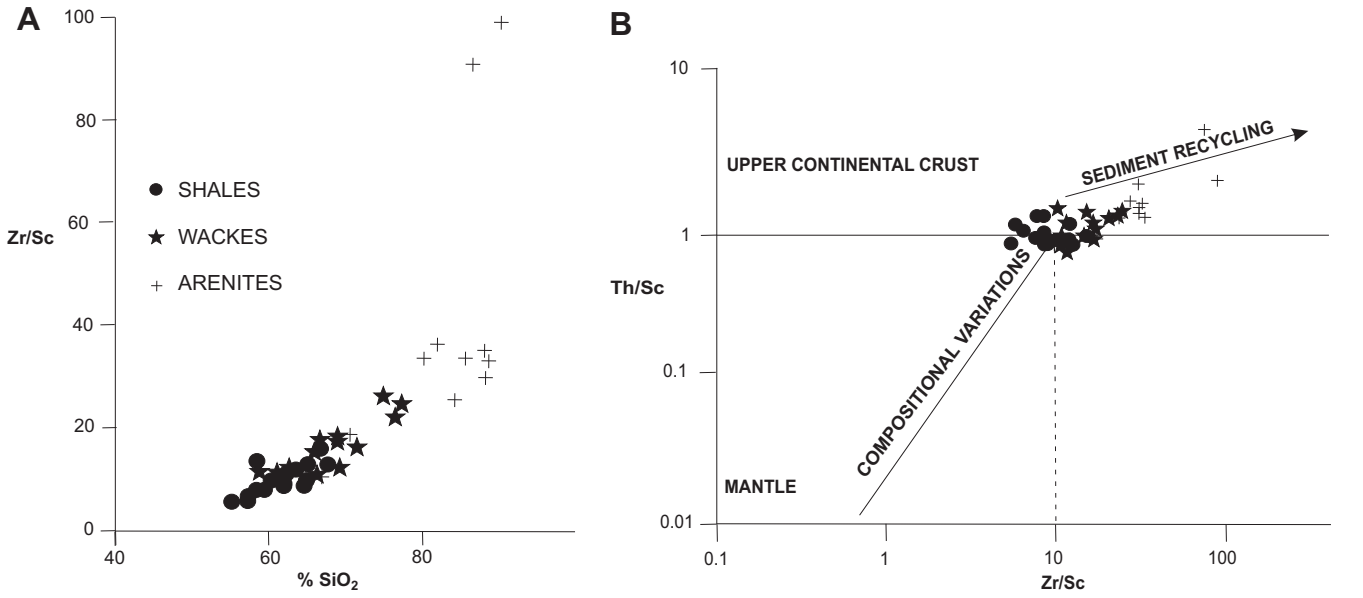

Fig. 14. Variation diagrams for immobile elements. A: Zr/Sc vs. SiO_2, B: Th/Sc vs. Zr/Sc (McLennan et al., 1990, 1993). These diagrams clearly show the more recycled character of arenites due to their higher Zr contents.

$Fe_2O_3 + MgO$ plot (Fig. 15B) the arenites correspond to the passive margins field and the wackes (with a considerable spread) are placed in the sectors of active continental margins and continental island arcs. In the scheme that compares the K_2O/Na_2O and SiO_2 values (Roser and Korsch, 1986, Fig. 15C) the samples studied plot within the fields of continental magmatic arcs and passive margins. However, it has already been noted that there is a lithological control on K_2O/Na_2O versus SiO_2 as shales are poorer in SiO_2 than the arenites but have maximum values of K_2O/Na_2O due to enrichment in illite. In the SiO_2/Al_2O_3 versus K_2O/Na_2O cross-plot (Maynard et al., 1982; Roser and Korsch, 1986; Gu et al., 2002) the wackes and shales correspond to the field of active continental margins whereas the arenites are very widely distributed across the field of passive continental margins owing to a large range in SiO_2/Al_2O_3 ratios (Fig. 15D). The huge variability in Cerro Agua Negra Formation sample compositions (even for shales) questions the validity of these diagrams as indicators of tectonic setting.

The La/Th versus Hf plot (Floyd and Leveridge, 1987; Fig. 16) shows that the analysed sandstones (wackes and arenites) are preferentially located in the area that corresponds to felsic and passive margin sources, with a high relative proportion of Th compared to La, and significant variations in Hf content that correspond both to recycled and non-recycled crustal materials.

The Th–Sc–Zr/10 ternary plot (Bhatia and Crook, 1986; Fig. 17A) tends to show important changes in provenance from Sc versus Th and Zr contents and in recycling through relative increase in Zr content. Cerro Agua Negra Formation arenites are located towards the Zr/10 apex, showing that they are the most recycled materials, as opposed to the wackes, which are in the centre of the plot. This impacts the tectonic interpretations, since the arenites correspond to the passive margin field, the wackes to the continental island arc field. A similar pattern can be seen in the La–Th–Sc diagram (Bhatia and Crook, 1986; Girty and Barber, 1993, Fig. 17B). This shows a comparatively high proportion of La (the most immobile component) relative to Th (of felsic origin) and Sc (of mafic origin). The arenites are shifted towards the La apex whereas the wackes are located within the field of continental island arcs as they have a relatively higher proportion of Sc.

Fig. 18 compares Ti/Zr and La/Sc ratios (Bhatia and Crook, 1986). The low values of Ti/Zr in the samples analysed indicate derivation from felsic rocks, with the range reflecting variations in the recycling process. Low values for the La/Sc ratio reveal relatively small proportions of the immobile La, which indicates a low level of recycling, except for a few arenites in which La/Sc is greater than 4. However, the number of samples with compositions indicating more unstable source areas or high mafic components is small, and most of them tend to be located in the active continental margin field. As shown by Gu et al. (2002), the discrimination between lithological types is quite good, as the shales are comparatively richer in Ti and in Sc, and the arenites (albeit with a high scatter) have higher values of the immobile elements Zr and La.

8. Discussion

Compositional analysis of the sedimentary rocks from the Cerro Agua Negra Formation helps interpret the origin (provenance and tectonic setting) of the deposits, but also raises questions about the applicability of commonly utilised discrimination plots and indices.

The sandstone petrography indicates a predominance of feldspathic litharenites throughout the formation. The compositional maturity is moderate and reveals that the sediment has been transported for a relatively short time and rapidly buried in an actively subsiding basin. Characteristics of the major detrital components suggest provenance from low-grade metamorphic, sedimentary and felsic plutonic terrains, with minor contribtions from volcanic sources. The parent rocks were exposed in tectonically uplifted regions located to the east of the Río Blanco basin (currently the Sierras Pampeanas and the Precordillera). Contributions from the Protoprecordilleran orogen (Qpch, Qmb, FKmb, Plgmb, B-Mmb, Ls, Lm; Table 2) indicates that the Protoprecordillera was still a positive relief area during the Pennsylvanian. Net and Limarino (2006) reached similar conclusions based on the study of modal analysis of Carboniferous units from

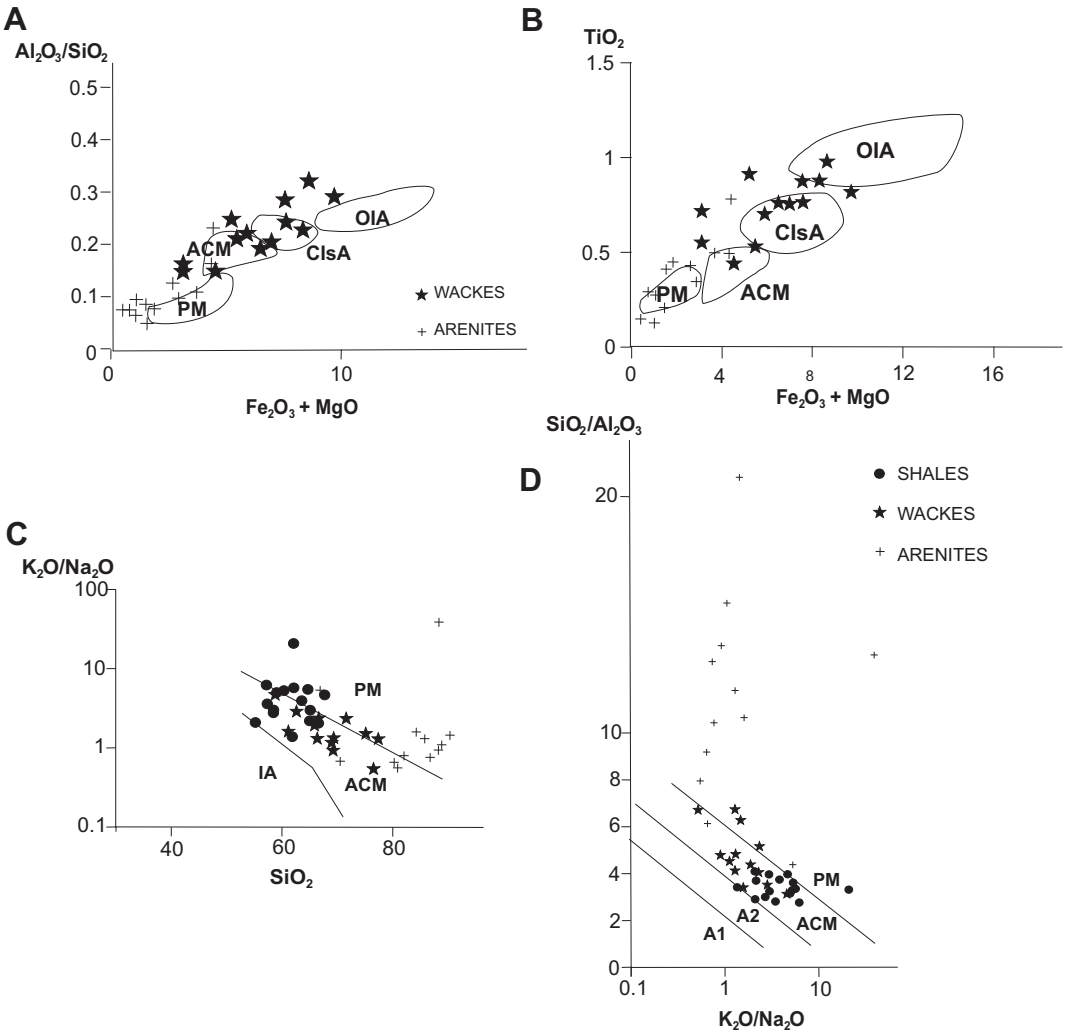

Fig. 15. Discrimination diagrams for tectonic settings based on the contents of major elements A: Al_2O_3/SiO_2 vs. $Fe_2O_3 + MgO$ (after Bhatia, 1983 for sandstones); B: TiO_2 vs. $Fe_2O_3 + MgO$ (Bhatia, 1983 for sandstones); C: K_2O/Na_2O vs. SiO_2 (after Roser and Korsch, 1986 for sandstones and shales); D: SiO_2/Al_2O_3 vs. K_2O/Na_2O (after Maynard et al., 1982; Roser and Korsch, 1986; Gu et al., 2002). Note the wide dispersion of the samples studied in all these diagrams. In the binary diagrams A and B only the samples of arenites and wackes were plotted. PM: passive margin. ACM: active continental margin. ClsA: continental island arc. OIA: oceanic island arc. IA: island arc.

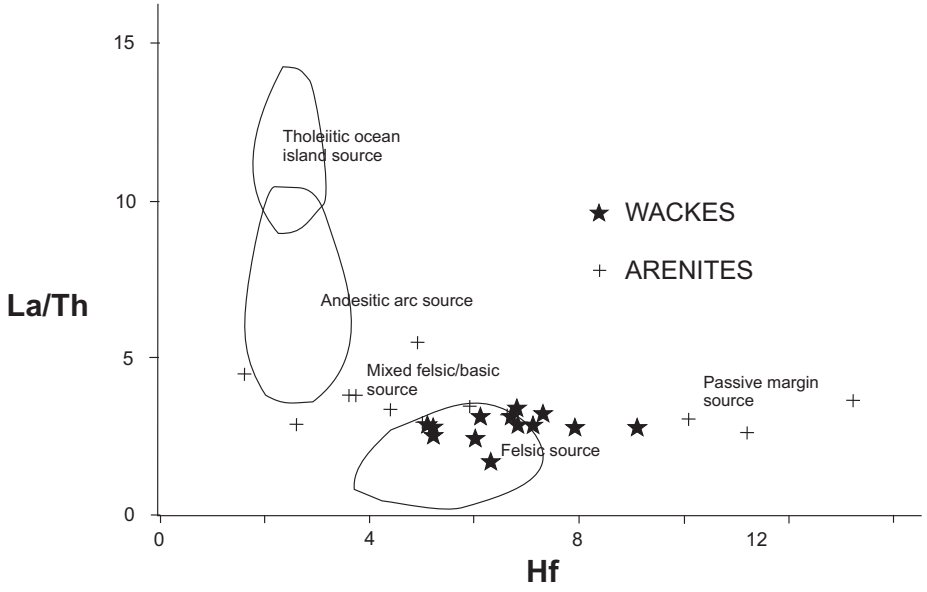

Fig. 16. Sandstone samples (arenites and wackes) from the Agua Negra Formation plotted on a La/Th vs. Hf diagram (Floyd and Leveridge, 1987).

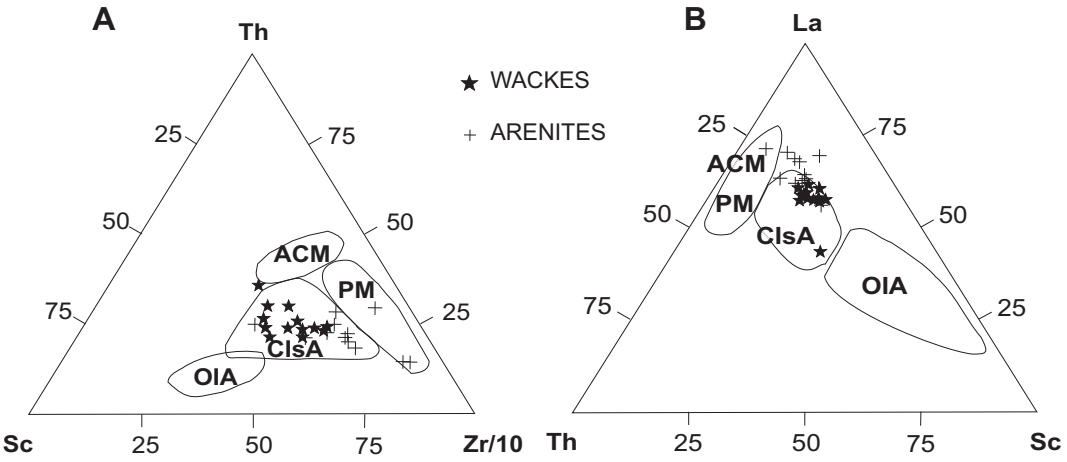

Fig. 17. Ternary tectonic interpretation diagrams for sandstones based on the proportions of immobile elements. A: Th–Sc–Zr/10 (Bhatia and Crook, 1986). B: La–Th–Sc (Bhatia and Crook, 1986; Girty and Barber, 1993). PM: passive margin. ACM: active continental margin. ClsA: continental island arc. OIA: oceanic island arc. The studied sandstone samples show a wide distribution; however, the arenites have greater contents of immobile elements (Zr, La) and plot towards the more stable source fields.

the Paganzo basin. They suggested a progressive decrease in relief of the Protoprecordillera after the Westphalian which led to the collapse of this orogen sometime around the Carboniferous–Permian transition.

The N–S trending block of the Protoprecordillera would have been cut by oblique and transverse valleys (approximately E–W) which served as sediment routing corridors between the Paganzo and the Río Blanco basins (Fig. 6). These allowed the sediment from the Pampean terrane to reach the Río Blanco basin, generating the mixed petrofacies of the Cerro Agua Negra Formation (Fig. 5). The small contribution of volcanic fragments demonstrates the limited importance of the Carboniferous volcanism as a supplier of both primary and reworked volcaniclastic material (cf. Limarino et al., 1996). Consequently there was no contribution from a magmatic arc during the deposition of the Cerro Agua Negra Formation. This negates previous interpretations of the Upper Carboniferous Río Blanco basin as a retroarc depression, with the development of a volcanic arc that closed it off towards the west (Azcuy and Caminos, 1988; Ramos and Palma, 1996). The new results suggest that the basin was open towards the proto-Pacific and it was floored by the rocks of the Chilenia terrane, after its collision with Gondwana (Fig. 6), in the Late Devonian–Early Carboniferous interval (Mpodozis and Kay, 1992).

The apparent lack of a magmatic arc west of the Río Blanco Basin is significant because several authors have proposed that a subduction-related magmatism took place during the late Palaeozoic along the western margin of Gondwana. In Chile, two N–S trending belts composed of the subduction-related granitoids are recognised. In the western flank of the high Andes, from 28°S southwards, this magmatism is represented by the Elqui Complex. A U–Pb zircon age of 285.7 ± 1.5 Ma (Guanta Tonalite) and a Rb–Sr whole rock isochron of 256 ± 10 Ma (Cochiguas Granodirite) have been obtained here (Pankhurst et al., 1996; Parada et al., 2007). Further west along the Coastal Cordillera of central Chile, Upper Palaeozoic granitoids extend for more than 750 km between latitudes 33° S and 38° S (Parada et al., 2007). Rb–Sr isochron ages of 292 ± 2 Ma and 308 ± 15 Ma (Hervé et al., 1988) and zircon U–Pb

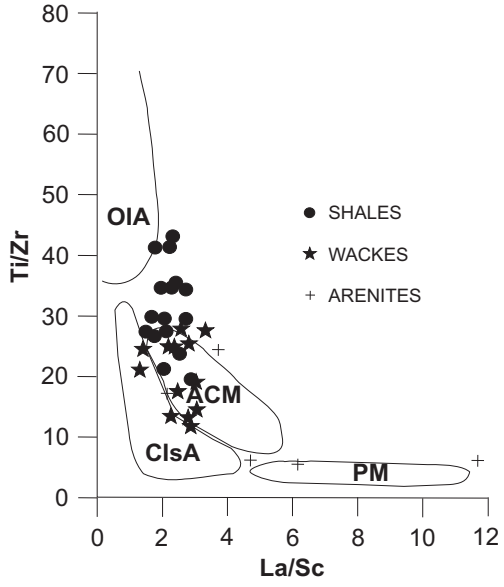

Fig. 18. Binary tectonic interpretation diagram for sandstones based on the Ti/Zr and La/Sc rations (Bhatia and Crook, 1986). Note the wide scatter of the samples from the Cerro Agua Negra Formation. PM: passive margin. ACM: active continental margin. ClsA: continental island arc. OIA: oceanic island arc. Once again the arenites have higher contents of immobile elements (La, Zr). As in the Cerro Agua Negra samples, Gu et al. (2002) indicated that fine-grained rocks are enriched in Sc and sandstones have larger values of La as a result of sorting.

Table 5
Areas of provenance for arenites, wackes and shales of the Cerro Agua Negra Formation according to commonly employed discrimination plots.

		Shale	Wacke	Arenite
Al_2O_3/SiO_2 vs. Fe_2O_3 + MgO	Fig. 15A		ACM-ClsA	PM (ACM)
TiO_2 vs. Fe_2O_3 + MgO	Fig. 15B		ACM-ClsA	PM (ACM)
K_2O/Na_2O vs. SiO_2	Fig. 15C	ACM-PM	ACM-PM	PM
SiO_2/Al_2O_3 vs. K_2O/Na_2O	Fig. 15D	ACM	ACM (PM)	PM
La/Th vs- Hf	Fig. 16		Felsic	Mixed Felsic–Basic to Passive Margin
Th–Sc–Zr/10	Fig. 17A		ClsA	ClsA-PM
La–Th–Sc	Fig. 17B		ClsA	ClsA-PM
Ti/Zr vs. La/Sc	Fig. 18	OIA-ACM	ACM-ClsA	ACM-PM

PM: Passive margin; ACM: active continental margin; ClsA: continental island arc; OIA: oceanic island arc.

ages of 309 and 290 Ma (Godoy and Loske, 1988) were reported for the northernmost granitoid complex of the Coastal Cordillera. Magmatic rocks of the Elqui Complex developed at the same latitude as the Río Blanco basin. However, their Permian ages post-date deposition of the Cerro Agua Negra Formation. Granitoids of the Coastal Cordillera have approximately the same age that the Cerro Agua Negra Formation, but they are not recorded at the latitude of the Río Blanco basin (around 30° S), only southwards of 33° S (Parada et al., 2007). Three scenarios may therefore be invoked: a) arc-related granitoids were not formed at the latitude of the Río Blanco basin, b) the plutonic rocks were being formed but remained in the subsurface during the Cerro Agua Negra deposition, and that there were no extrusive rocks associated with this arc-related magmatism, and c) the Coastal Cordillera was not part of western Gondwana but was part of the exotic Pichidangui terrane and was docked to Gondwana after the Late Palaeozoic times (Forsythe et al., 1987).

The geochemical data show that the Cerro Agua Negra Formation rocks are similar in composition to the UCC (Figs. 11, 13, 14 and 16), although with a modest enrichment of SiO_2 in the arenites and of Al_2O_3 and K_2O in the shales. The latter is a factor of source rock weathering but also of mesogenetic formation of secondary minerals, especially illite, which was concentrated in the clay fraction of the deposits. Variations in CIA values of the different lithologies show that this parameter serves as a reliable indicator of the proportion of clay minerals in the case of wackes and shales. In contrast, the arenites have lower CIA values, even though they are richer in stable SiO_2.

The rare earth elements show a similar pattern to that of average terrigenous contributions, being characterised by relative enrichment of the light-REE, depletion of the heavy-REE and a significant negative Eu anomaly. The comparatively higher values of Zr in the arenites reflects a sorting effect and a greater level of recycling, possibly due to the tendency for zircon grains to be concentrated in the psammitic fractions.

One of the key observations from the geochemical study is that major element and several trace element contents vary systematically with sedimentary rock texture, even for some elements traditionally considered to be “immobile”. Gu et al. (2002), Armstrong-Altrin et al. (2004) and Pe-Piper et al. (2008) also found changes in geochemical composition that can be explained by grain-size variations in terrigenous rocks. The largest differences are always between arenites and shales, while the wackes present intermediate values. This calls into question the use of variation diagrams that aimed at showing differences in provenance and in the tectonic setting of source areas and sedimentary basins. Table 5 compares the results of the main discrimination diagrams for Cerro Agua Negra Formation samples and shows that these plots give a wide range of tectonic/source area interpretations for the same samples. Arenites plot essentially in the passive margin fields of provenance, though some samples are placed in the continental island arc and the active continental margin fields. Shales are located in variable fields, but always in very unstable provenance lithologies, such as oceanic island arcs, continental island arcs and the active continental margins. In turn, wacke samples fall in intermediate positions, mainly between the continental island arc to the active continental margin fields.

The conclusions reached in the study of the Cerro Agua Negra Formation are critical and open a question as to the use of geochemistry as an indicator of origin, recycling and tectonism. So, the generalised attempt to apply interpretative diagrams related to these aspects and based on the contents of certain chemical elements or on relations between them may not be successful if other lines of geological, stratigraphic and sedimentological research are not simultaneously borne in mind. To the effects of the multiple interactions between origin, weathering, transport and diagenesis on sedimentary geochemistry (McLennan, 1989; Cox and Lowe, 1996; Armstrong-Altrin et al., 2004) it is important to add the potential influence of the textural types of siliciclastic rocks that make up the geological units that are the object of study.

9. Conclusions

The sandstones of the Cerro Agua Negra Formation show a fairly homogeneous composition dominated by low-grade metamorphic and sedimentary rock fragments. This is reflected in the predominance of feldspathic litharenites and to a lesser extent litharenites. The results and interpretations help constrain the Late Carboniferous palaeogeography of the Río Blanco Basin and the provenance of the Cerro Agua Negra Formation. The low degree of compositional variability in the sandstones and the presence of a significant proportion of unstable lithic fragments, imply a relatively high rate of erosion of the source areas, along with a short residence time of the clastic material in the surface environment. Mineralogical compositions, the features of the sandstone grains and the detrital modes indicate multiple contributions from the Proto-precordillera (main source area) and the Sierras Pampeanas blocks. Minor contributions of volcanogenic grains highlight a limited importance of contemporaneous volcanism (cf. Limarino et al., 1996). Therefore, the existence of a volcanic arc to the west of the basin is unlikely.

Major and trace element compositions of arenites, wackes and shales in the Cerro Agua Negra Formation are similar to the average UCC values, although with enrichment of SiO_2 in the arenites. Relatively high proportions of Al_2O_3, K_2O, Fe_2O_3 and MgO in the shales can be attributed to their higher content in clay minerals, and therefore the CIA produces higher values in the shales, which are enriched in Al_2O_3. The rare earth elements reflect terrigenous contributions, since there is relative enrichment of the light elements, a negative anomaly of Eu and a relative depletion of the heavy rare earth elements. The arenites have higher contents of Zr than the shales, which suggest a tendency towards preferential concentration of detrital zircon in sands and a potentially longer history of reworking.

The geochemical composition of the Cerro Agua Negra rocks, including the proportions of immobile elements, is strongly dependent of grain-size (sandstones-shales) and sorting (arenites-wackes). The differences are greatest when arenites and shales are compared, while the wackes have intermediate values. For this reason the variation diagrams traditionally used to define provenance and tectonism of the source areas and of the sedimentary basins are ineffective in this study. These conclusions question the use of geochemistry as an indicator of origin, recycling and tectonism when texture of the sedimentary rocks is not taken into consideration.

Acknowledgements

The authors wish to express their gratefulness to Pedro Busquets and Miguel López by their helpful comments. Special thanks to Jim Hendry whose thoughtful comments and review helped improve the manuscript. We acknowledge constructive suggestions made by two anonymous reviewers. The work was supported by grant CGL2009-13706-C03-03 (Ministerio de Educación y Ciencia and Ministerio de Ciencia e Innovación, Spain) and by the Grup de Qualitat 2009-SGR-1198 (Generalitat de Catalunya, Spain).

Appendix. Chemical composition of the Cerro Agua Negra rocks

Shales

	XFAN 3	XFAN 6	XFAN 8	XFAN 11	XFAN 13	XFAN 14	XFAN 16	XFAN 19	XFAN 22	XFAN 23	XFAN 24	XFAN 25	XFAN 26	XFAN 29	XFAN 30	XFAN 36
SiO_2 (%)	65.03	58.45	63.49	62.09	62.1	67.66	62.05	60.2	57.35	55.14	58.49	66.72	59.22	64.56	57.21	64.95
Al_2O_3 (%)	16.4	17.94	16.88	18.85	18.56	17.04	18.12	18.12	20.43	19.04	19.54	16.28	18.86	17.64	21.01	17.45
Fe_2O_3(T) (%)	6.06	7.38	6.64	6.97	6.4	4.35	6.62	7.67	7.6	11.48	6.3	4.95	7.51	6.41	8.98	6.95
MnO (%)	0.069	0.073	0.069	0.027	0.033	0.029	0.081	0.105	0.115	0.131	0.095	0.048	0.078	0.095	0.101	0.061
MgO (%)	2.38	3	2.62	1.41	2.05	1.33	2.49	3.62	1.97	2.51	1.82	1.42	2.9	2.3	2.89	2.01
CaO (%)	0.44	0.5	0.34	0.28	0.48	0.27	0.87	0.3	0.32	0.74	0.91	0.41	0.28	0.32	0.48	0.67
Na_2O (%)	1.26	1.23	1.09	0.19	0.71	0.76	2.53	0.68	1.01	1.14	1.44	1.5	0.86	0.72	0.71	1.37
K_2O (%)	3.8	3.74	4.29	4.1	4.09	3.63	3.51	3.63	3.58	2.43	3.96	3.21	4.36	3.98	4.48	3.03
TiO_2 (%)	0.982	0.943	0.986	0.897	0.943	0.884	0.845	0.943	0.976	0.907	0.858	0.859	0.829	0.704	0.916	0.863
P_2O_5 (%)	0.19	0.21	0.2	0.17	0.21	0.17	0.18	0.17	0.15	0.18	0.08	0.11	0.15	0.12	0.18	0.1
LOI (%)	3.82	4.97	3.41	5.36	5.15	4.76	3.05	4.57	4.8	4.68	6.2	4.14	3.79	3.45	4.01	3.45
Total (%)	100.4	98.43	100	100.4	100.7	100.9	100.3	100	98.31	98.37	99.69	99.63	98.82	100.3	101	100.9
Sc (ppm)	17	20	18	20	19	17	16	17	21	23	18	16	18	16	21	18
Be (ppm)	5	4	4	5	5	3	4	4	4	4	3	3	4	3	4	3
V (ppm)	136	142	145	184	153	146	116	121	159	169	112	104	134	113	152	138
Ba (ppm)	583	572	553	625	566	514	655	762	692	524	738	673	762	803	884	624
Sr (ppm)	40	32	35	59	42	32	98	19	70	102	105	92	74	82	77	107
Y (ppm)	32	34	36	29	38	32	29	32	37	35	23	38	34	34	39	36
Zr (ppm)	220	160	215	180	207	220	146	162	141	132	242	260	145	143	127	175
Cr (ppm)	90	80	80	90	90	110	60	80	90	90	40	70	80	90	100	70
Co (ppm)	14	19	17	8	10	9	10	16	18	21	12	16	16	22	23	20
Ni (ppm)	30	30	20	<20	<20	<20	<20	30	<20	40	30	<20	30	40	40	30
Cu (ppm)	20	40	30	20	40	10	80	40	30	50	<10	30	30	10	30	<10
Zn (ppm)	70	100	100	110	90	90	100	30	120	80	50	50	80	70	50	<30
Ga (ppm)	23	22	20	24	22	20	20	31	25	24	24	21	20	22	28	20
Ge (ppm)	2	<1	1	2	3	1	2	2	1	2	2	2	1	2	2	2
As (ppm)	35	26	16	25	27	19	11	198	<5	9	32	8	25	19	22	21
Rb (ppm)	195	172	167	221	152	186	132	129	149	167	169	156	185	182	203	149
Nb (ppm)	16	16	13	14	15	14	14	17	15	16	17	14	14	12	16	14
Mo (ppm)	<2	<2	<2	<2	<2	<2	<2	<2	<2	<2	<2	<2	<2	<2	<2	<2
Ag (ppm)	<0.5	<0.5	<0.5	<0.5	<0.5	<0.5	<0.5	<0.5	3.5	<0.5	<0.5	<0.5	<0.5	<0.5	<0.5	<0.5
In (ppm)	<0.2	<0.2	<0.2	<0.2	<0.2	<0.2	<0.2	<0.2	<0.2	<0.2	<0.2	<0.2	<0.2	<0.2	<0.2	<0.2
Sn (ppm)	7	6	2	4	2	6	3	3	2	6	2	4	9	6	12	12
Sb (ppm)	1.5	<0.5	0.7	<0.5	<0.5	<0.5	<0.5	1.8	<0.5	<0.5	1.3	<0.5	1.2	<0.5	<0.5	<0.5
Cs (ppm)	17.2	12.4	19.3	12.9	15.6	14.3	11	5	9.5	30.6	9.9	14.1	15.7	12.4	12	8.9
La (ppm)	29.9	48.2	38.5	33.8	29.1	42.8	31.7	39.4	47	40.8	37.3	46.2	49.3	43.6	49.2	37.1
Ce (ppm)	66.7	101	80.1	70.1	57.6	92.7	69.8	91.4	99.4	94.6	79	95.6	105	101	116	86.9
Pr (ppm)	7.41	11.8	9.46	7.95	8.16	11.1	8.14	10.2	11.5	10.7	9.77	11.5	11.4	11.3	13	9.89
Nd (ppm)	25.9	40	33.3	25.7	28.9	37.4	28.2	35.7	38.5	36.3	32.9	41	39.8	38.3	43.8	33.3
Sm (ppm)	5.5	8.1	7.3	5.5	6.3	8	6	7.4	8.5	7.3	6.7	8.7	7.9	7.4	8.9	7.2
Eu (ppm)	1.29	1.63	1.4	1.08	1.36	1.55	1.08	1.48	1.7	1.79	1.33	1.72	1.57	1.4	1.78	1.46
Gd (ppm)	5	7.2	6.7	5	5.9	6.5	5.1	6.4	7	6.8	5.2	7.2	7.2	7.1	8.1	6.6
Tb (ppm)	0.9	1.1	1.1	0.8	1	1	0.8	1.2	1.1	1.1	0.9	1.2	1.1	1.1	1.3	1.1
Dy (ppm)	6.2	6.1	6.2	4.8	6.2	6.2	4.7	7	6.4	6.4	5.5	7.3	6.6	6.3	7.2	6.5
Ho (ppm)	1.3	1.2	1.2	1	1.2	1.3	0.9	1.3	1.3	1.3	1.1	1.5	1.3	1.3	1.5	1.4
Er (ppm)	3.9	3.6	3.7	3.1	3.9	3.8	2.7	3.6	4	4.2	3.1	4.6	3.9	3.8	4.3	4.1
Tm (ppm)	0.59	0.52	0.56	0.48	0.58	0.58	0.44	0.53	0.6	0.65	0.46	0.67	0.6	0.56	0.65	0.61
Yb (ppm)	3.9	3.3	3.6	3.2	3.7	3.7	2.9	3.3	3.9	4.1	3.1	4.1	3.8	3.6	4	3.8
Lu (ppm)	0.59	0.5	0.57	0.49	0.53	0.54	0.4	0.48	0.57	0.64	0.45	0.63	0.52	0.54	0.61	0.56
Hf (ppm)	5.8	5.2	6	5.3	5.6	7	4	4.7	4.4	4.4	8	7.9	4.8	4.6	4.5	5.5
Ta (ppm)	1.4	1.6	1.4	1.4	1.6	1.7	1.5	1.8	1.5	1.6	1.7	1.5	1.4	1.3	1.5	2.1
Tl (ppm)	0.9	1	1.2	1.7	1.1	1.2	1	0.2	1	0.8	0.9	1.4	1	0.8	0.7	0.2
Pb (ppm)	7	11	17	13	<5	23	10	<5	9	8	<5	19	15	9	<5	<5
Bi (ppm)	<0.4	<0.4	<0.4	<0.4	0.5	5.7	0.7	<0.4	<0.4	<0.4	<0.4	<0.4	1.1	<0.4	<0.4	1.9
Th (ppm)	12.9	15	12.8	16.3	14.1	15.5	11.2	11.9	17.6	16.1	12.1	12.4	19	16.7	19.4	13
U (ppm)	3	2.9	2.9	4.5	4.9	3.7	4.2	2.8	5.1	5.8	4	4.3	3.3	3.8	3.3	3.6

WACKES

	XFAN 4	XFAN 15	XFAN 17	XFAN 20	XFAN 21	XFAN 27	XFAN 28	XFAN 31	XFAN 32	XFAN 37	XFAN 38	XFAN 39	XFAN 40
SiO_2 (%)	65.87	76.47	69.02	66.64	58.77	66.34	62.63	71.45	69.21	61.02	68.92	77.27	75
Al_2O_3 (%)	15.05	11.45	14.48	16.58	18.82	16.15	17.88	13.77	14.33	17.86	15.15	11.58	12.03
Fe_2O_3(T) (%)	5.92	3.36	4.01	4.19	7.06	5.4	5.76	4.83	5.3	7.72	4.39	2.27	2.54
MnO (%)	0.063	0.071	0.067	0.066	0.095	0.136	0.09	0.057	0.13	0.089	0.08	0.036	0.029
MgO (%)	2.4	1.15	1.46	1.02	1.53	2.19	1.8	1.67	1.68	1.98	1.49	0.83	0.59
CaO (%)	0.58	1.4	1.01	0.61	0.48	1.42	0.42	0.36	1.83	0.95	1.19	1.48	1.37
Na_2O (%)	1.7	2.93	3.29	1.12	0.72	2.05	1.28	1.22	1.81	1.7	1.87	1.58	1.59

(*continued*)

	XFAN 4	XFAN 15	XFAN 17	XFAN 20	XFAN 21	XFAN 27	XFAN 28	XFAN 31	XFAN 32	XFAN 37	XFAN 38	XFAN 39	XFAN 40
K_2O (%)	3.28	1.56	3.02	2.67	3.37	2.69	3.68	2.93	2.39	2.71	2.16	2.05	2.42
TiO_2 (%)	0.871	0.433	0.525	0.912	0.972	0.759	0.865	0.763	0.744	0.81	0.694	0.54	0.708
P_2O_5 (%)	0.2	0.14	0.16	0.2	0.14	0.19	0.11	0.15	0.13	0.07	0.15	0.06	0.1
LOI (%)	3.21	1.15	1.39	5.2	6.35	2.23	4.6	2.56	2.28	3.61	3.07	2.61	2.54
Total (%)	99.14	100.1	98.43	99.2	98.3	99.55	99.12	99.75	99.82	98.52	99.17	100.3	98.91
Sc (ppm)	16	10	13	16	20	15	17	11	13	17	13	10	11
Be (ppm)	4	2	3	3	4	4	<1	<1	3	4	3	2	2
V (ppm)	139	65	84	124	138	105	104	70	91	114	93	81	106
Ba (ppm)	603	252	705	587	539	640	726	498	610	467	397	420	472
Sr (ppm)	61	130	122	83	80	180	81	73	149	144	170	109	124
Y (ppm)	30	21	25	35	48	34	37	28	28	35	32	22	27
Zr (ppm)	247	220	234	284	233	164	210	179	159	195	240	246	290
Cr (ppm)	70	40	40	80	90	60	80	70	60	60	50	30	30
Co (ppm)	26	52	30	24	21	15	14	18	20	23	21	23	16
Ni (ppm)	30	<20	<20	30	30	30	30	30	20	30	<20	<20	<20
Cu (ppm)	20	10	<10	20	20	20	30	20	20	20	40	30	60
Zn (ppm)	100	50	60	80	120	60	50	60	70	120	70	50	30
Ga (ppm)	20	11	17	21	23	17	22	17	18	22	18	12	11
Ge (ppm)	2	<1	1	2	1	1	1	1	1	2	2	1	1
As (ppm)	18	45	37	12	7	8	38	10	7	34	20	6	12
Rb (ppm)	139	80	111	127	166	134	122	111	150	138	119	113	122
Nb (ppm)	15	8	10	16	15	12	14	12	13	15	12	9	11
Mo (ppm)	<2	<2	<2	<2	<2	<2	<2	<2	<2	<2	<2	<2	<2
Ag (ppm)	<0.5	<0.5	<0.5	<0.5	<0.5	<0.5	<0.5	<0.5	<0.5	<0.5	<0.5	<0.5	<0.5
In (ppm)	<0.2	<0.2	<0.2	<0.2	<0.2	<0.2	<0.2	<0.2	<0.2	<0.2	<0.2	<0.2	<0.2
Sn (ppm)	3	7	6	4	2	5	2	2	5	5	6	3	10
Sb (ppm)	1.9	<0.5	<0.5	1.4	<0.5	1.1	<0.5	<0.5	<0.5	<0.5	<0.5	1.5	1.8
Cs (ppm)	15.3	3.6	8.5	10.3	15.2	13.5	8.6	5.6	11.2	13.9	8.3	7.5	7.9
La (ppm)	21.4	28.9	30.2	48.7	45	49.6	24.7	30.9	34	40.8	32.4	28.5	33.9
Ce (ppm)	46.9	61.3	63.9	97.1	94.6	108	51.7	63.6	81.1	91.5	75.8	62.4	67.9
Pr (ppm)	5.73	7.29	7.73	11	11.4	11.7	6.7	8.4	9.06	10.6	8.92	7.13	7.11
Nd (ppm)	21.1	24.2	26.5	37.8	42.1	39.2	23.3	28.3	30.5	36.9	31.1	25.1	24
Sm (ppm)	4.7	4.8	5.7	7.6	9.3	8	5.1	5.9	6.2	7.8	6.8	5.1	5
Eu (ppm)	0.95	0.93	1.23	2.09	2.01	1.51	1.1	0.98	1.13	1.89	1.72	1.15	1.01
Gd (ppm)	4.3	4.2	4.8	6	8.7	7.2	5.3	5.4	5.9	7.1	6.5	4.6	5
Tb (ppm)	0.8	0.6	0.7	1	1.4	1.1	1	0.9	0.9	1.1	1	0.7	0.8
Dy (ppm)	5.6	3.7	4.5	6.6	8.6	6.3	6.1	5.4	5.3	6.4	5.7	4.3	4.9
Ho (ppm)	1.2	0.8	1	1.4	1.7	1.3	1.2	1.1	1.1	1.3	1.1	0.9	1
Er (ppm)	3.7	2.4	2.9	3.9	5	3.7	3.6	3	3.4	3.6	3.4	2.7	3.3
Tm (ppm)	0.57	0.36	0.44	0.62	0.74	0.56	0.53	0.43	0.49	0.52	0.5	0.42	0.5
Yb (ppm)	3.8	2.3	2.7	4.1	4.7	3.6	3.4	2.7	3	3.3	3.2	2.7	3.2
Lu (ppm)	0.56	0.33	0.39	0.6	0.67	0.48	0.52	0.41	0.46	0.51	0.46	0.4	0.5
Hf (ppm)	6.3	6.8	6.7	7.3	6.8	5.1	6	5.2	5.2	6.1	7.1	7.9	9.1
Ta (ppm)	1.7	3.9	2.7	1.6	1.5	1.4	1.6	1.5	1.7	1.9	1.9	2.4	2
Tl (ppm)	1	0.5	0.8	1	1.2	0.9	0.4	0.6	1.1	1.2	0.8	1	1
Pb (ppm)	12	<5	7	13	11	42	<5	5	10	15	11	10	14
Bi (ppm)	0.8	<0.4	<0.4	0.8	<0.4	0.6	<0.4	<0.4	<0.4	<0.4	3	1.8	3.2
Th (ppm)	12.7	10	9.7	15.1	13.4	17.4	10.3	12.2	12.3	13.1	11.4	10.4	12.5
U (ppm)	3.1	2.5	2.2	4.9	5.7	3.4	3.7	2.9	3	2.7	2.8	3	3.7

ARENITES

	XFAN 1	XFAN 2	XFAN 5	XFAN 7	XFAN 9	XFAN 10	XFAN 12	XFAN 18	XFAN 33	XFAN 34	XFAN 35	XFAN 41
SiO_2 (%)	81.91	88.09	88.67	85.69	84.25	66.97	88.27	80.78	86.63	80.17	70.52	90.17
Al_2O_3 (%)	7.88	6.46	5.73	7.29	7.93	15.42	6.65	10.2	6.68	8.73	11.49	4.33
Fe_2O_3(T) (%)	2.09	0.3	0.75	1.12	0.82	2.93	0.54	1.84	1.47	2.85	3.49	1.28
MnO (%)	0.04	0.003	0.015	0.009	0.005	0.035	0.007	0.023	0.026	0.05	0.115	0.02
MgO (%)	0.79	0.15	0.26	0.37	0.24	1.48	0.23	0.8	0.36	0.83	0.84	0.25
CaO (%)	0.71	0.12	0.1	0.15	0.2	0.43	0.03	0.45	0.61	0.83	4	0.13
Na_2O (%)	2.14	1.34	1.49	1.24	1.23	0.36	0.05	2.71	1.81	2.14	1.92	0.74
K_2O (%)	1.68	1.25	1.62	1.63	1.99	1.98	2.03	1.5	1.36	1.39	1.28	1.08
TiO_2 (%)	0.335	0.143	0.113	0.198	0.265	0.775	0.281	0.422	0.44	0.491	0.487	0.402
P_2O_5 (%)	0.1	0.06	0.05	0.06	0.08	0.25	0.03	0.27	0.07	0.05	0.07	0.04
LOI (%)	0.87	1	0.36	1.15	1.42	8.11	1.23	1.4	0.44	0.86	4.45	0.95
Total (%)	98.55	98.91	99.15	98.92	98.43	98.74	99.35	100.4	99.9	98.4	98.67	99.4
Sc (ppm)	6	3	2	4	6	18	5	5	5	7	9	4
Be (ppm)	2	1	<1	<1	<1	2	1	2	<1	2	2	<1
V (ppm)	36	17	12	22	36	153	32	36	29	58	94	24
Ba (ppm)	292	150	262	162	231	311	111	253	304	255	293	209
Sr (ppm)	86	24	46	24	31	331	10	48	110	80	142	31

(*continued on next page*)

(*continued*)

	XFAN 1	XFAN 2	XFAN 5	XFAN 7	XFAN 9	XFAN 10	XFAN 12	XFAN 18	XFAN 33	XFAN 34	XFAN 35	XFAN 41
Y (ppm)	18	5	7	12	16	17	14	39	18	17	20	14
Zr (ppm)	218	105	66	134	153	189	148	412	454	235	169	395
Cr (ppm)	<20	<20	<20	<20	<20	150	20	30	<20	30	30	20
Co (ppm)	29	53	45	37	48	9	31	29	58	41	24	37
Ni (ppm)	<20	<20	30	<20	<20	40	<20	<20	30	30	<20	20
Cu (ppm)	<10	<10	<10	<10	<10	60	<10	<10	<10	<10	10	<10
Zn (ppm)	<30	<30	<30	<30	<30	40	<30	<30	<30	40	40	<30
Ga (ppm)	7	6	6	7	9	20	8	11	7	9	12	4
Ge (ppm)	<1	1	<1	<1	<1	2	2	<1	1	1	1	<1
As (ppm)	<5	<5	21	11	11	32	89	62	<5	<5	14	12
Rb (ppm)	52	53	47	67	85	119	93	74	48	70	71	34
Nb (ppm)	8	4	3	5	7	13	5	9	8	8	7	6
Mo (ppm)	<2	<2	<2	<2	<2	<2	<2	<2	<2	<2	<2	<2
Ag (ppm)	<0.5	<0.5	<0.5	<0.5	<0.5	<0.5	<0.5	<0.5	<0.5	<0.5	<0.5	<0.5
In (ppm)	<0.2	<0.2	<0.2	<0.2	<0.2	<0.2	<0.2	<0.2	<0.2	<0.2	<0.2	<0.2
Sn (ppm)	4	6	3	7	9	7	2	4	7	3	4	2
Sb (ppm)	<0.5	<0.5	1.1	<0.5	<0.5	1.6	2.6	0.5	1.1	0.8	<0.5	1.1
Cs (ppm)	2.3	1.6	1.5	5.2	3	17	3.6	3.1	1.9	10.7	6.7	1.7
La (ppm)	21.5	10.9	15.2	17.9	20.6	67.1	24.9	58.7	30.7	24.3	19.7	18.9
Ce (ppm)	45.1	23.6	28.2	35.8	42.5	151	49.6	117	64.5	54.9	46.5	41.2
Pr (ppm)	5.32	2.7	3	4.16	4.95	20.8	5.46	13.7	7.6	5.86	5.63	4.55
Nd (ppm)	18.6	8.6	10	13	15.7	58.2	17.2	46.5	24.9	20.6	20	15.5
Sm (ppm)	4	1.6	1.8	2.5	3.2	9.8	3.4	9.3	4.9	4.2	4.3	3
Eu (ppm)	0.79	0.34	0.41	0.51	0.74	1.69	0.62	1.58	0.91	0.83	0.95	0.55
Gd (ppm)	3.4	1.4	1.5	2.2	2.9	6.4	2.6	7.9	3.7	3.7	4.1	2.7
Tb (ppm)	0.5	0.2	0.2	0.3	0.5	0.9	0.4	1.3	0.7	0.6	0.6	0.4
Dy (ppm)	3.3	1.1	1.5	2.1	2.6	4.7	2.7	7.9	4	3.4	3.6	2.5
Ho (ppm)	0.7	0.2	0.3	0.4	0.5	0.8	0.6	1.5	0.8	0.7	0.7	0.5
Er (ppm)	2.2	0.8	0.9	1.3	1.7	2.4	1.8	4.4	2.2	2.1	2.2	1.5
Tm (ppm)	0.33	0.13	0.14	0.22	0.27	0.37	0.28	0.64	0.33	0.31	0.33	0.25
Yb (ppm)	2.1	0.9	0.9	1.4	1.8	2.5	1.8	4.1	2.1	2	2.1	1.7
Lu (ppm)	0.3	0.13	0.13	0.21	0.27	0.4	0.27	0.59	0.32	0.28	0.32	0.25
Hf (ppm)	5.9	2.6	1.6	3.6	4.4	4.9	3.7	10.1	13.2	6.6	5	11.2
Ta (ppm)	2.6	4.3	3.3	3.3	4	1.4	2.6	2.9	4.4	3.8	1.8	3.9
Tl (ppm)	0.4	0.4	0.3	0.4	0.4	1.4	1.4	0.5	0.2	0.7	0.5	0.2
Pb (ppm)	9	<5	7	<5	<5	12	<5	6	<5	6	15	<5
Bi (ppm)	<0.4	<0.4	1.1	0.4	0.4	3.3	12	1.1	<0.4	<0.4	3.2	0.7
Th (ppm)	6.2	3.8	3.4	4.7	6.1	12.2	6.6	19.2	8.4	7.7	6.7	7.2
U (ppm)	1.7	0.7	0.6	1	1.3	4.9	1.3	3.4	1.8	1.7	2	1.5

References

Amos, A.J., Rolleri, E., 1965. El Carbónico marino en el valle Calingasta-Uspallata, San Juan-Mendoza. Boletín de Informaciones Petroleras 368, 50–71.

Aparicio, E.P., 1969. Contribución al conocimiento de la edad de los sedimentos del arroyo de Agua Negra, Departamento de Iglesia, San Juan. Revista de la Asociación Geológica Argentina 31, 190–193.

Archangelsky, S., Azcuy, C.L., González, C.R., Sabattini, N., 1987. Paleontología, bioestratigrafía y paleoecología de las cuencas Paganzo, Calingasta – Uspallata y Río Blanco. In: Archangelsky, S., Amos, A.J., Andreis, R.R., Azcuy, C.L., González, C.R., López Gamundí, O., Sabattini, N. (Eds.), El Sistema Carbonífero en la República Argentina. Academia Nacional de Ciencias, Córdoba, pp. 133–151.

Armstrong-Altring, J.S., Verma, S.P., 2005. Critical evaluation of six tectonic setting discrimination diagrams using geochemical data of Neogene sediments from know tectonic settings. Sedimentary Geology 177, 115–129.

Amstrong-Altrin, J.S., Lee, Y.I., Verma, S.P., Ramasamy, S., 2004. Geochemistry of sandstones from the Upper Miocene Kudankulam Formation, southern India: implications for provenance, weathering, ant tectonic setting. Journal of Sedimentary Research 74, 285–297.

Asiedu, D.K., Suzui, S., Shibata, T., 2000. Provenance of sandstones from the Lower Cretaceous Sasayama Group, inner zone of southwest Japan. Sedimentary Geology 131, 9–24.

Asiedu, D.K., Dampare, S.B., Asmoah Sakyi, P., Banoeng-Yakubo, B., Osae, S., Nyarko, B.J.B., Manu, J., 2004. Geochemistry of Paleoproterozoic metasedimentary rocks from the Birim diamontiferous field, southern Ghana: implications for provenance and crustal evolution at the Archean–Proterozoic boundary. Geochemical Journal 38, 215–228.

Azcuy, C.L., Caminos, R., 1988. Características paleogeográficas y diastróficas de algunas cuencas paleozoicas de América del Sur: una reseña. Boletín Sociedad Geológica de Perú 78, 203–224.

Barone, M., Dominici, R., Muto, F., Critelli, S., 2008. Detrital modes in a Late Miocene wedge-top basin, northeastern Calabria, Italy: compositional record of wedge-top partitioning. Journal of Sedimentary Research 78, 693–711.

Bhatia, M.R., 1983. Plate tectonics and geochemical composition of sandstones. Journal of Geology 92, 181–193.

Bhatia, M.R., Crook, A.W., 1986. Trace element characteristics of graywackes and tectonic setting discrimination of sedimentary basins. Contributions to Mineralogy and Petrology 92, 181–193.

Blatt, H., Middleton, G., Murray, R., 1980. Origin of Sedimentary Rocks. Prentice-Hall Inc, Englewood Cliffs, 782 pp.

Boles, J.R., Franks, S.G., 1979. Clay diagenesis in Wilcox Sandstones of southwest Texas: implications of smectite diagenesis on sandstone cementation. Journal of Sedimentary Petrology 49, 55–70.

Busquets, P., Colombo, F., Heredia, N., Solé de Porta, N., Rodríguez Fernández, L.R., Álvarez Marrón, J., 2005. Age and tectonostratigraphic significance of the Upper carboniferous series in the basement of the Andean Frontal Cordillera: geodynamic implications. Tectonophysics 399, 181–194.

Cahill, T., Isacks, B.L., 1992. Seismicity and the shape of the subducted Nazca plate. Journal of Geophysical Research 97, 17503–17529.

Césari, S.N., Gutiérrez, P.R., 2000. Palynostratigraphy of Upper Paleozoic sequences in central-western Argentina. Palynology 24, 113–146.

Chung, F.H., 1974. Quantitative interpretation of X-ray diffraction patterns of mixtures. I. Matrix flushing method for quantitative multicomponent analysis. Journal of Applied Crystallography 7, 519–525.

Cox, R., Lowe, D.R., 1996. Quantification of the effects of secondary matrix on the analysis of sandstone composition, and a petrographic–chemical technique for retrieving original framework grain modes of altered sandstones. Journal of Sedimentary Research 66, 548–558.

Critelli, S., Ingersoll, R.V., 1996. Interpretation of neovolcanic versus paleovolcanic sand grains: an example from Miocene deep marine sandstones of the Topanga Group (Southern California). Sedimentology 42, 783–804.

Desjardins, P.R., Buatois, L.A., Limarino, C.O., Cisterna, G.A., 2009. Latest Carboniferous–earliest Permian transgressive deposits in the Paganzo Basin of western Argentina: Lithofacies and sequence stratigraphy of a coastal-plain to bay succession. Journal of South American Earth Sciences 28, 40–53.

Dickinson, W.R., 1970. Interpreting detrital modes of graywacke and arkose. Journal of Sedimentary Petrology 40, 695–707.

Dickinson, W.R., Suczek, C.A., 1979. Plate tectonics and sandstone composition. American Association of Petroleum Geologists Bulletin 63, 2164–2182.

Dickinson, W.R., Valloni, R., 1980. Plate tectonics and provenance of sands in modern ocean basins. Geology 8, 82–86.

Dickinson, W.R., Beard, L.S., Brakenridge, G.R., Erjavec, J.L., Ferguson, R.C., Inman, K.F., Knepp, R.A., Lindberg, F.A., Ryberg, P.T., 1983. Provenance of North American Phanerozoic sandstones in relation to tectonic setting. Geological Society of America Bulletin 94, 222–235.

Fielding, C.R., Frank, T.D., Isbell, J.L., 2008. The late Paleozoic ice age – a review of current understanding and synthesis of global climate patterns. In: Fielding, C.R., Frank, T.D., Isbell, J.L. (Eds.), Resolving the Late Paleozoic Ice Age in Time and Space. Geological Society of America Special Publication 441, pp. 343–354. Boulder.

Floyd, P.A., Leveridge, B.E., 1987. Tectonic environment of the Devonian Gramscatho basin, south Cornwall: framework mode and geochemical evidence from turbiditic sandstones. Journal of the Geological Society of London 144, 531–542.

Floyd, P.A., Winchester, J.A., Park, R.G., 1989. Geochemistry and tectonic setting of Lewisian clastic metasediments from the Early Proterozoic Loch Maree Group of Gairloch, NW Scotland. Precambrian Research 45, 203–214.

Floyd, P.A., Franke, W., Shail, R., Dörr, W., 1990. Provenance and depositional environment of Thenohercynian synorogenic greywacke from the Giessen nappe, Germany. Geologische Rundschau 79, 611–626.

Folk, R.L., Andrews, P.B., Lewis, D.W., 1970. Detrital sedimentary rock classification and nomenclature for use in New Zealand. New Zealand Journal of Geology and Geophysics 13, 937–968.

Forsythe, R.D., Kent, D.V., Mpodozis, C., Davidson, J., 1987. Paleomagnetism of Permian and Triassic rocks, central Chilean Andes. In: McKenzie, G.A. (Ed.), Structure, Tectonics and Geophysics. Geophysical Monograph 40. American Geophysical Union, pp. 241–251.

Gazzi, P., 1966. Le arenarie del flysch sopracretaceo dell`Appennino modenese; correlazioni con il flysch di Monghidoro. Mineralogica et Petrographic Acta 12, 69–97.

Girty, G.H., Barber, R.W., 1993. REE, Th and Sc evidence for the depositional setting and source rock characteristics of the Quartz Hill chert, Sierra Nevada, California. In: Johnsson, J.M., Basu, A. (Eds.), Processes Controlling the Composition of Clastic Sediments. Geological Society of America, Special Paper 284, pp. 109–119.

Godoy, E., Loske, W., 1988. Tectonismo sinplutónico de dioritas jurásicas al sur de Valparaiso: datos U–Pb sobre la Fase Quintay. Revista Geológica de Chile 15, 119–127.

González, C.R., 1977. *Oriocrassatella* y *Stutchburia* (Bivalvia) en la ingresión marina del Pérmico inferior de la Quebrada de Agua Negra, provincia de San Juan (Argentina). Ameghiniana 13, 127–140.

Gu, X.X., Liu, J.M., Zheng, M.H., Tang, I.X., Qi, L., 2002. Provenance and tectonic setting of the Proterozoic turbidites in Hunan, south China: geochemical evidence. Journal of Sedimentary Research 72, 393–407.

Henry, L.C., Isbell, J.L., Limarino, C.O., 2008. Carboniferous glacigenic deposits of the Protoprecordillera of west central Argentina. In: Fielding, C.R., Frank, T.D., Isbell, J.L. (Eds.), Resolving the Late Paleozoic Ice Age in Time and Space. Geological Society of America Special Publication 441, pp. 131–142. Boulder.

Heredia, N., Rodríguez Fernández, L.R., Gallastegui, G., Busquets, P., Colombo, F., 2002. Geological setting of the Argentine Frontal Cordillera in the flat-slab segment (30°00′–31°30′ S latitude). Journal of South American Earth Sciences 15, 79–99.

Herron, M.M., 1988. Geochemical classification of terrigenous sands and shales from core or log data. Journal of Sedimentary Petrology 58, 820–829.

Hervé, F., Munizaga, F., Parada, M.A., Brook, M., Pankhurst, R.J., Snelling, N.J., Drake, R., 1988. Granitoids of the Coast Range of central Chile: geochronology and geologic setting. Journal of South American Earth Sciences 1, 185–194.

Höy, T., 1976. Calc-silicate isograds in the Riondel area, southeastern British Columbia. Canadian Journal of Earth Sciences 13, 1093–1104.

Ingersoll, R., Cavazza, W., 1991. Reconstruction of Oligo-Miocene volcaniclastic dispersal patterns in north-central New Mexico using sandstone petrofacies. SEPM Special Publication 45, pp. 227–236.

Jafarzadeh, M., Barzi, M.H., 2008. Petrography and geochemistry of Ahwaz Sandstone Member of Asmari Formation, Zagros, Iran: implications on provenance and tectonic setting. Revista Mexicana de Ciencias Geológicas 25, 247–260.

Lamaskin, T.A., Dorsey, R.J., Vervoort, J.D., 2008. Tectonic controls on mudrock geochemistry, Mesozoic rocks of eastern Oregon and western Idaho, U.S.A.: implications for cordilleran tectonics. Journal of Sedimentary Research 78, 765–783.

Limarino, C.O., Spalletti, L., 2006. Paleogeography of the upper Paleozoic basins of southern South America: An overview. Journal of South American Earth Sciences 22, 134–155.

Limarino, C.O., César, S.N., Net, L.I., Manenssi, S.A., Gutiérrez, R.P., Tripaldi, A., 2002. The Upper Carboniferous postglacial transgression in the Paganzo and Río Blanco basins (northwestern Argentina): facies and stratigraphic significance. Journal of South American Earth Sciences 15, 445–460.

Limarino, C.O., Tripaldi, A., Marenssi, S., Fauqué, L., 2006. Tectonic, sea-level, and climatic controls on Late Paleozoic sedimentation in the western basins of Argentina. Journal of South American Earth Sciences 22, 205–226.

Maynard, J.B., Valloni, R., Yu, H., 1982. Composition of modern deep sea sands from arc-related basins. Geological Society of London, Special Publication 10, pp. 551–561. Londres.

McLennan, S.M., 1989. Rare earth elements in sedimentary rocks: influence of provenance and sedimentary processes. Reviews in Mineralogy 21, 169–200.

McLennan, S.M., 2001. Relationships between the trace element composition of sedimentary rocks and upper continental crust. Geochemistry, Geophysics, Geosystems 2 paper number 2000GC000109.

McLennan, S.M., Taylor, S.R., 1984. Archean sedimentary rocks and their relation to the composition of the Archean continental crust. In: Kröner, A., Hanson, G.N., Goodwin, A.M. (Eds.), Archean Geochemistry. Springer, Berlin and Heidelberg, pp. 47–72.

McLennan, S.M., Taylor, S.R., 1991. Sedimentary rocks and crustal evolution: tectonic setting and secular trends. Journal of Geology 99, 1–21.

McLennan, S.M., Nance, W.B., Taylor, S.R., 1980. Rare earth element–thorium correlations in sedimentary rocks, and the composition of the continental crust. Geochimica et Cosmochimica Acta 44, 1833–1840.

McLennan, S.M., Taylor, S.R., McCulloch, M.T., Maynard, J.B., 1990. Geochemical and Nd–Sr isotopic composition of deep-sea turbidites: crustal evolution and plate tectonic associations. Geochimica et Cosmochimica Acta 54, 2015–2050.

McLennan, S.M., Hemming, S.R., McDaniel, D.K., Hanson, G.N., 1993. Geochemical Approaches to Sedimentation, Provenance, and Tectonics. Geological Society of America, Special Paper 284, pp. 21–40.

Moore, D.M., Reynolds Jr., R.C., 1989. X-Ray Diffraction and the Identification and Analysis of Clay Minerals, 332 pp.. Oxford University Press, Oxford.

Mpodozis, C., Kay, S.M., 1992. Late Paleozoic to Triassic evolution of the Gondwana margin: evidence from Chilean Frontal Cordilleran Batholiths (28°S to 31°S). Geological Society of America, Bulletin 104, 999–1014.

Nakamura, N., 1974. Determination of REE, Ba, Fe, Mg, Na and K in carbonaceous and ordinary chondrites. Geochimica et Cosmochimica Acta 38, 757–773.

Nesbitt, H.W., Young, G.M., 1982. Early Proterozoic climates and plate motions inferred from major element chemistry of lutites. Nature 299, 715–717.

Nesbitt, H.W., Young, G.M., McLennan, S.M., Keays, R.R., 1996. Effects of chemical weathering and sorting on the petrogenesis of siliciclastic sediments, with implications for provenance studies. Journal of Geology 104, 525–542.

Net, L.I., Limarino, C.O., 2006. Applying sandstone petrofacies to unravel the Upper Carboniferous evolution of the Paganzo Basin, northwest Argentina. Journal of South American Earth Sciences 22, 239–254.

Pankhurst, R.J., Millar, I.L., Hervé, F., 1996. A Permo-Carboniferous U–Pb age for the part of the Guanta unit of the Elqui-Limarí batholith at Río del Tránsito, northern Chile. Revista Geológica de Chile 23, 35–42.

Parada, M.A., López Escobar, L., Olivero, V., Fuentes, F., Morata, D., Calderón, M., Aguirre, L., Féraud, G., Espinoza, F., Moreno, H., Figueroa, O., Muñoz Bravo, J., Troncoso Vásquez, R., Stern, C.R., 2007. Andean magmatism. In: Moreno, T., Gibbons, W. (Eds.), The Geology of Chile. Geological Society of London, London, pp. 115–146.

Pe-Piper, G., Triantafyllidis, S., Piper, D.J.W., 2008. Geochemical identification of clastic sediment provenance from known sources of similar geology: the Cretaceous Scotian Basin, Canada. Journal of Sedimentary Research 78, 595–607.

Pérez Loinaze, V.S., Limarino, C.O., César, S.N., 2010. Glacial events in Carboniferous sequences from Paganzo and Río Blanco basins (northwest Argentina): palynology and depositional setting. Geologica Acta (en prensa).

Pittman, E.D., 1963. Use of zoned plagioclase as an indicator of provenance. Journal of Sedimentary Petrology 33, 380–386.

Polanski, J., 1970. Carbónico y Pérmico de la Argentina, 216 pp. Editorial Universitaria de Buenos Aires, Buenos Aires.

Ramos, V.A., Cristallini, E.O., Pérez, D.J., 2002. The Pampean flat-slab of the Central Andes. Journal of South American Earth Sciences 15, 59–78.

Ramos, V., Palma, M.A., 1996. Tectónica. In: Archangelsky, S. (Ed.), El Sistema Pérmico en la República Argentina y en la República Oriental de Uruguay. Academia Nacional de Ciencias, Córdoba, pp. 239–254.

Reineck, H.E., Wunderlich, F., 1968. Classification and origin of flaser and lenticular bedding. Sedimentology 11, 99–104.

Rodríguez Fernández, L.R., Heredia, N., Marín, G., Quesada, C., Robador, A., Ragona, D., Cardó, R., 1996. Tectonoestratigrafía y estructura de los Andes Argentinos entre los 30°30′ y 31°00′ de latitud Sur. Actas XIII Congreso Geológico Argentino 2, 111–124.

Rodríguez Fernández, L.R., Heredia, N., Espina, R.G., Cegarra, M.I., 1999. Estratigrafía y estructura de los Andes Centrales argentinos entre los 30° y 31° de latitud Sur. Acta Geológica Hispánica 32, 93–102.

Roser, B.P., Korsch, R.J., 1986. Determination of tectonic setting of sandstone–mudstone suites using SiO_2 content and K_2O/Na_2O ratio. Journal of Geology 94, 635–650.

Roser, B.P., Cooper, R.A., Nathan, S., Tulloch, A.J., 1996. Reconnaissance sandstone geochemistry, provenance, and tectonic setting of the Lower Paleozoic terranes of the West Coast and Nelson, New Zealand. New Zealand Journal of Geology and Geophysics 39, 1–16.

Ryan, K.M., Williams, D.M., 2007. Testing the reliability of discrimination diagrams for determining the tectonic depositional environment of ancient sedimentary basins. Chemical Geology 242, 103–125.

Salfity, J.A., Gorustovich, S.A., 1983. Paleogeografía de la cuenca del Grupo Paganzo (Paleozoico Superior). Revista de la Asociación Geológica Argentina 38, 437–453.

Scasso, R.A., Limarino, C.O., 1997. In: Petrología y Diagénesis de Rocas Clásticas. Asociación Argentina de Sedimentología, Buenos Aires, Publicación Especial 1, 259 pp.

Taylor, S.R., McLennan, S.M., 1981. The composition and evolution of the continental crust: rare earth element evidence from sedimentary rocks. Philosophical Transactions of the Royal Society of London A301, 381–399.

Taylor, S.R., McLennan, S.M., 1985. The Continental Crust: Its Composition and Evolution, 312 pp. Blackwell, Londres.

Taylor, S.R., Rudnick, R.L., McLennan, S.M., Eriksson, K.A., 1986. Rare earth element patterns in Archean high-grade metasediments and their tectonic significance. Geochimica et Cosmochimica Acta 50, 2267–2279.

Tortosa, A., Palomares, M., Arribas, J., 1991. Quartz grain types in Holocene deposits from the Spanish Central System; some problems in provenance analysis. In: Morton, A.C., Todd, S.P., Haughton, P.D.W. (Eds.), Developments in Sedimentary Provenance Studies. Geological Society, Special Publication 57, pp. 47–54. Londres.

Vujovich, G.I., Kay, S.M., 1998. A Laurentian? Grenville-age oceanic arc/back-arc terrane in the Sierra de Pie de Palo, Western Sierras Pampeanas, Argentina. In: Pankhurst, R.J., Rapela, C.W. (Eds.), The Proto-Andean Margin of Gondwana. Geological Society, Special Publication 142, pp. 159–179. Londres.